VISUAL AND PHOTOGRAPHIC FLOW PATTERN STUDIES DURING CONDENSATION INSIDE HORIZONTAL TUBES

by

HASSAN MOHAMED HASSAN SOLIMAN

B.Sc., Assiut University, U.A.R., 1966

A MASTER'S THESIS

submitted in partial fulfillment of the

requirements for the degree

MASTER OF SCIENCE

Department of Mechanical Engineering

KANSAS STATE UNIVERSITY

Manhattan, Kansas

1970

Approved by:

M. J. Azer

Major Professor

TABLE OF CONTENTS

THIS BOOK CONTAINS NUMEROUS PAGES WITH MULTIPLE PENCIL AND/OR PEN MARKS THROUGHOUT THE TEXT.

THIS IS THE BEST IMAGE AVAILABLE.

TABLE OF CONTENTS continued

LIST OF FIGURES

LIST OF FIGURES continued

LIST OF PLATES

LIST OF TABLES

CHAPTER I

INTRODUCTION

Two-phase flow occurs in a large number of practical engineering devices. The two phases may be of the same substance, such as liquid and its vapor, or two completely different substances. Evaporation and condensation in boilers and condensers of a steam power plant, air-conditioning and refrigeration equipment, and components of distillation and water purification plants, as well as cooling of nuclear reactors are applications in which two-phase, one-component flow occurs. Applications in which two-phase, two-component flow takes place are: pumping of mixtures of oil and natural gas, hydraulic conveying of wheat, pulvarized coal and ores, and material handling in food processing.

The successful design and operation of equipment handling two-phase systems depends on the understanding of the flow hydrodynamics. The ultimate objective of a successful design being the accurate prediction of overall macroscopic performance characteristics such as pressure drop and heat and mass transfer coefficients. It has been established that one- or two-component, two-phase flow can adjust itself in a variety of flow regimes or patterns. Knowing the flow pattern of two-phase flow is very important in terms of modelling analytically the flow situation. An analytic technique which is adequate for one flow pattern may be meaningless in another. The flow patterns are usually studied by visual or photographic means.

Early studies of two-phase flow were directed towards the understanding of the hydrodynamic aspects of adiabatic, two-phase, two-component (gas and liquid) flow. In spite of the complexities inherent in the hydrodynamics of this problem, due to the immense number of independent variables involved, such studies lead to a great deal of information on flow patterns, phase distribution, and pressure drop. If two-phase flow is associated with heat transfer, the hydrodynamics of the flow become more complicated. This is due to the fact that heat transfer causes phase changes and changes in phase distribution and flow pattern. In such a case, there is a definite interdependence between heat transfer characteristics and local flow conditions. There is also one additional factor that adds to the complexity of diabatic two-phase flows. In adiabatic flow the flow can become fully developed over the entire flow path, while on the other hand, the flow can never become fully developed in diabatic flow. As a result, local descriptions of flow become insufficient without knowledge of the previous history of the flow.

Despite the added complexities of heat transfer, several experimental and simplified analytical sutides have been conducted with some success to diabatic two-phase flow problems mainly in forced convection boiling. There is some incomplete information in the literature on flow patterns, phase distribution, and heat transfer characteristics.

Through literature survey of two-phase flow, the author became aware of the fact that an important area of diabatic two-phase flow was ignored by investigators. No information could be found

on flow pattern, phase distribution during condensation. Most analytical studies on condensation, reported in literature, were based on the assumption that a certain flow pattern existed without reference to the conditions under which such a pattern can exist. In a few other cases, flow pattern was assumed on the basis of the criteria developed for adiabatic flow. Also, many empirical and semi-empirical relations are available in the literature for predicting heat transfer coefficients and pressure drop for condensation inside tubes without reference to the flow pattern for which they can be applied. A correlation which is applicable to one flow pattern may be useless in another. Each available correlation must be identified with a certain flow pattern.

The objective of this investigation is to visually and photographically study the flow patterns during forced convection condensation inside a horizontal tube, under different flow conditions, with the ultimate objective of establishing the criteria that distinguishes one flow pattern from another.

TWO-PHASE FLOW PATTERNS

Flow pattern is the most important parameter in two-phase flow because the hydrodynamic behavior of two-phase flow differs in various flow patterns. To know the flow pattern is as important as to know whether the flow is laminar or turbulent in single-phase flow. This investigation will be concerned with the flow pattern of two-phase flow where the components are the vapor and liquid phases during condensation.

Two-phase flows are classified by the vapor-liquid distribution. There are three basic modes of vapor-liquid distributions in both adiabatic and diabatic flows:

1. Bubbles suspended in the liquid stream.
2. Liquid droplets suspended in the vapor stream.
3. Liquid and vapor existing intermittently.

The typical combinations of these modes as they develop in flow channels are called flow patterns. Figure 1 shows a schematic drawing of the flow patterns in horizontal adiabatic two-phase flow. These flow patterns can develop in the following order by changing the flow from single-phase liquid flow to single-phase gas flow, by increasing the gas flow rate: Bubbly, plug, straitified, slug, wavy, annular, and spray flows. For adiabatic two-phase flow there is a rather complete agreement between investigators in the descriptions of these patterns; they may disagree only in the name given to them. For example, spray flow is frequently called "fog or dispersed" flow and the transition from slug to annular is frequently called "churn" flow. The description given by Alves [1]*, for the different flow patterns of adiabatic two-phase (gas and liquid) flow inside horizontal tubes, appears to be the most complete one, and the most accepted in the literature of two-phase flow.

The Following is a summary of Alves' [1] descriptions of the different flow patterns:

---

*Numbers in brackets refer to references in bibliography.

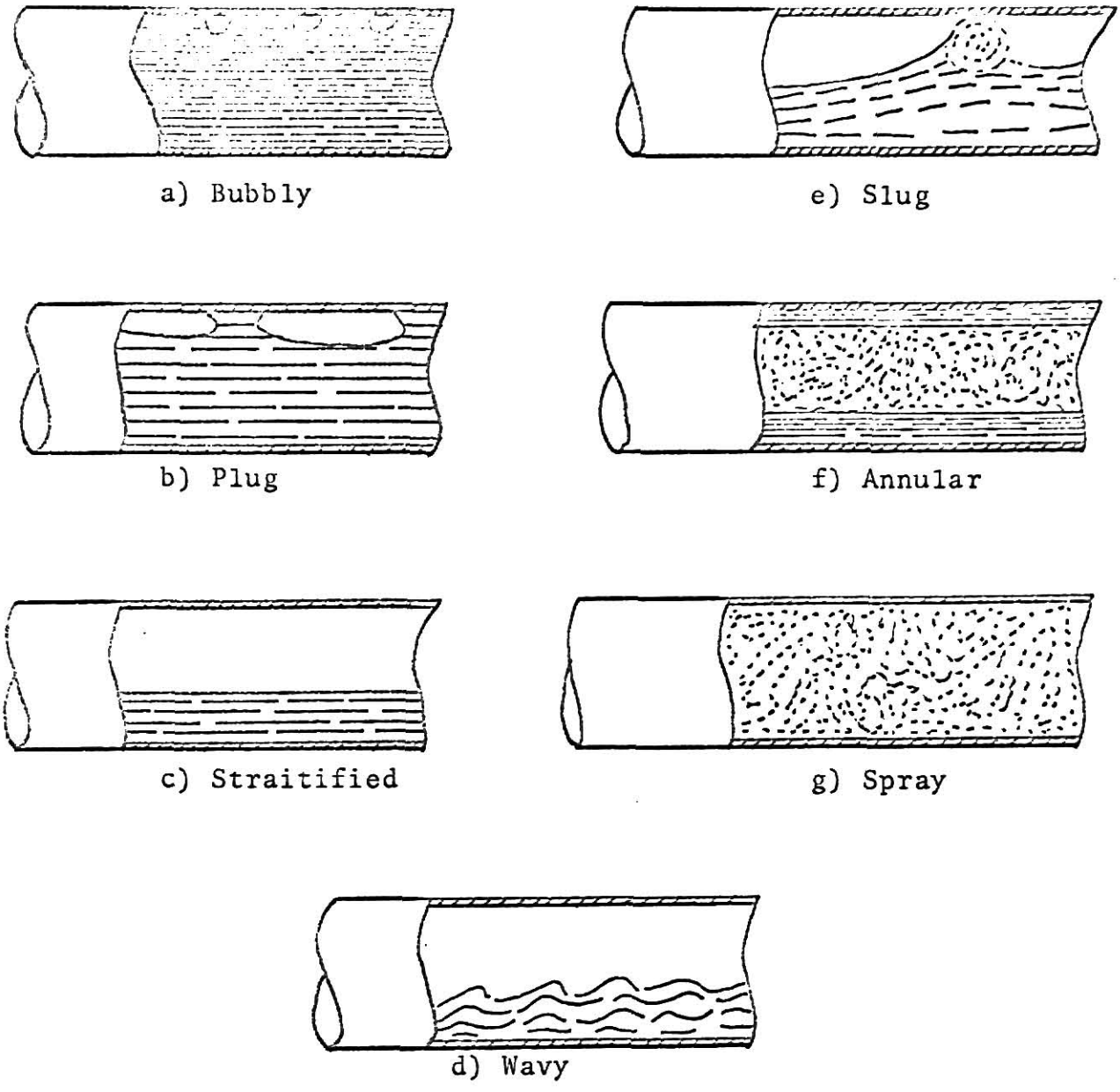

Fig. 1. Observed Flow Patterns by Alves [1], in Adiabatic Horizontal Flow.

(a) Bubbly flow:

Flow in which bubbles of gas move along the upper part of the pipe at approximately the same velocity as the liquid.

(b) Plug flow:

Flow in which alternate plugs of liquid and gas move along the upper part of the pipe.

(c) Straitified flow:

Flow in which liquid flows along the bottom of the pipe and the gas above it over a smooth interface.

(d) Wavy flow:

Flow which is similar to straitified flow except that the gas moves at a higher velocity and the interface is disturbed by waves travelling in the direction of the flow.

(e) Slug flow:

Flow in which a wave is picked up periodically by the more rapidly moving gas to form a frothy slug which passes through the pipe at a much greater velocity than the average liquid velocity. These slugs can cause a highly fluctuating pressure characteristics and sometimes cause dangerous vibrations in the equipment.

(f) Annular flow:

Flow in which the liquid flows in a film around the inside wall of the pipe and the gas flows at a higher velocity at the core.

(g) Spray flow:

Flow in which most or nearly all of the liquid is entrained as a spray by the gas.

Figure 2 shows a schematic diagram of the flow patterns in adiabatic two-phase vertical upflow. By changing the flow from single-phase liquid flow to single-phase gas flow and by increasing the gas flow rate, these flow patterns can develop in the following order:

(a) Homogeneous bubble flow, where homogeneous bubbles are suspended in the liquid stream.

(b) Non-homogeneous bubble flow, where bubbles start to grow in size in a random fashion.

(c) Slug flow, where bubbles coalesce forming smooth Taylor bubbles.*

(d) Semiannular flow, where the bubbles break down forming a continuous unstable column of gas in the core.

(e) Same as (d).

(f) Annular flow, where the gas flows in the core while the liquid flows in a continuous film around the tube.

(g) Spray-Annular flow, where part of the film breaks into droplets and becomes entrained in the gas core.

(h) Mist flow, where all the liquid phase is entrained as droplets in the gas.

It is to be noticed that, due to the change in orientation of the tube, from the horizontal to the vertical position, both the stratified and the wavy flows of the horizontal flow do not appear in vertical upflow. This is due to gravity effects.

---

*For the definition of Taylor bubbles, the reader is referred to reference [10].

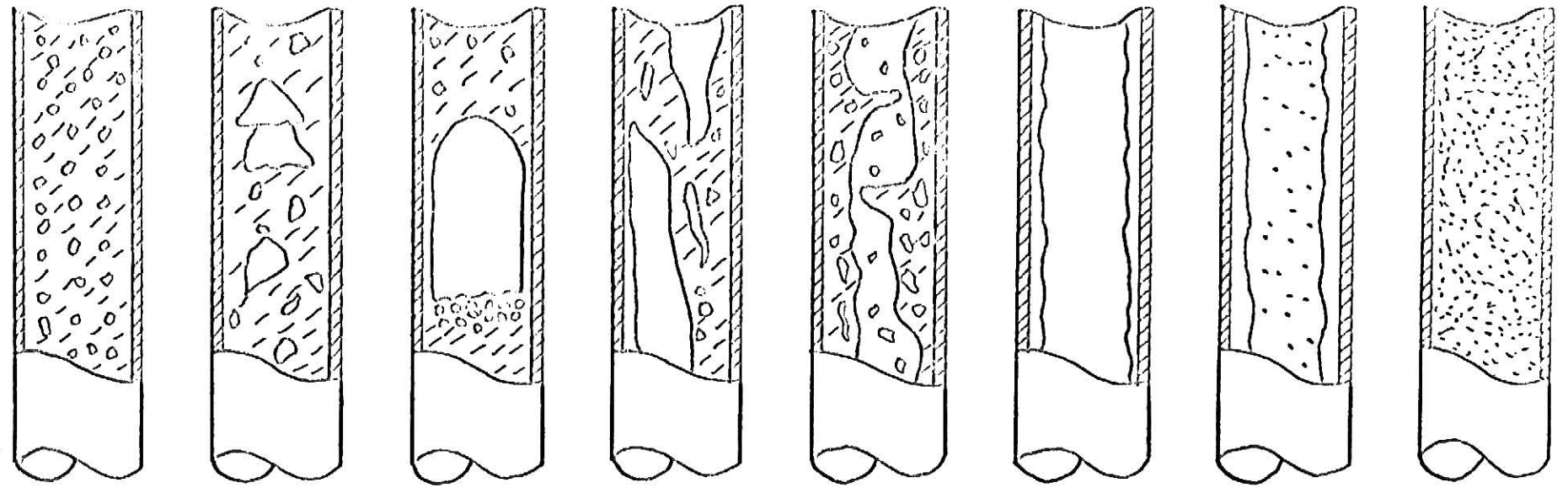

Fig. 2. Schematic Drawings of Flow Patterns in Adiabatic Two-Phase Vertical Upflow.

Figure 3 shows a schematic diagram of flow patterns in two-phase vertical upflow with heat transfer. These flow patterns were reported by investigators concerned with the heat transfer characteristics during forced convection boiling.

Thus far, it has become obvious that the orientation, and whether the flow is adiabatic or diabatic, plays a significant part in the development of the flow patterns of two-phase flow. It is the objective of this investigation to cast some light on the flow patterns that can develop during condensation inside a horizontal tube.

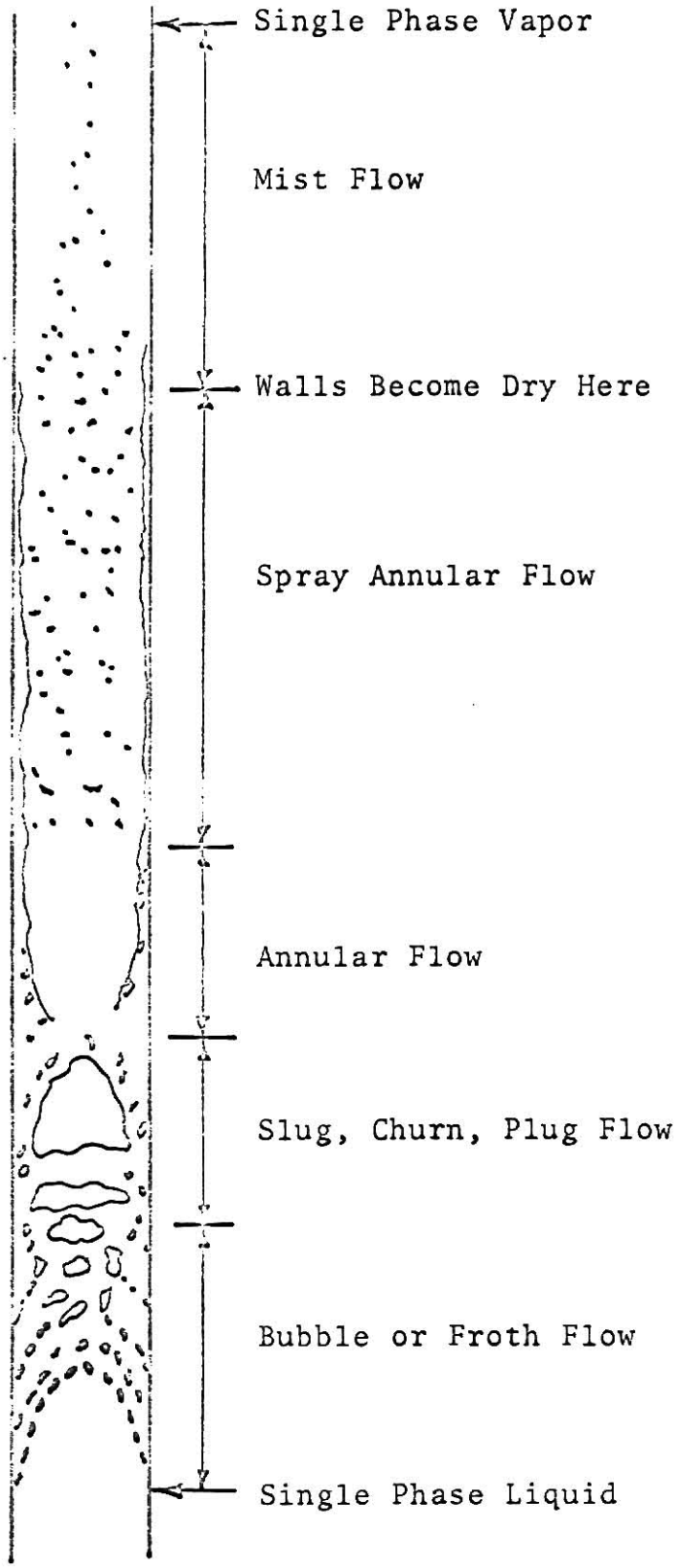

Fig. 3. Schematic Drawing of Flow Patterns in Two-Phase Vertical Upflow with Heat Transfer.

CHAPTER II

LITERATURE SURVEY

Early flow pattern studies of two-phase flow were concerned with systems where the two-phase moving stream was a mixture of a gas and a liquid. More recent studies were concerned with diabatic two-phase flow, as in forced convection boiling of upflow inside tubes, where heat addition causes a continuous change in the flow pattern. Accordingly, the literature survey will be divided into two main parts, namely:

1. Literature survey on flow patterns of adiabatic two-phase flow.
2. Literature survey on flow patterns of diabatic two-phase flow.

Adiabatic Two-Phase Flow

Experimental investigations conducted in the area of adiabatic two-phase flow covered flow in ducts of different geometries (circular and rectangular), different orientations (horizontal and vertical), and broadly covered all practical ranges of velocities, flow rates, and working fluids.

Martinelli and Coworkers [2,3] and Lockhart and Martinelli [4], reported the earliest information about two-phase flow patterns. The main concern of their investigations was the estimation of the pressure drop of air-water mixtures flowing inside ducts. They did not examine the hydrodynamics of the flow within each flow pattern or the limiting conditions for the existence of these

patterns.

Alves [1] observed the flow patterns of adiabatic flow of water-air, and oil-air mixtures in a 1 in.diam., 19 ft. long glass tube at atmospheric pressure. He observed the flow patterns illustrated in Fig. 1. Alves also constructed a flow pattern map, based on plotting the liquid superficial velocity versus the gas velocity, showing transition lines between the different flow patterns.

Bergelin and Gazley [5] reported classifications for the flow patterns, similar to those of Alves [1], for the flow of water-air mixtures. However, they did not make any distinctions between bubbly and plug flows. In addition, Bergelin and Gazley [5] considered the bubbly, wavy, and slug flow patterns as unsteady ones, because they were accompanied by high pressure fluctuations, while they considered the annular flow as steady with respect to time and axial direction. Also, they considered straitified flow as steady with respect to time but unsteady with respect to distance in the axial direction. This was due to its sensitivity to any type of vibration or external disturbance. Bergelin and Gazley presented their data by constructing a flow pattern map based on plotting the air flow rate versus the water flow rate. On their map they identified the transition lines between the different flow regimes. Such a map is only applicable to air-water mixtures flowing inside 1 in. diameter tubes at atmospheric pressure.

Hoogendoorn [6] extended the work of his predecessors to cover different pipe diameters and a wider range of velocities. He

observed the same flow patterns reported by Alves [1] and Bergelin and Gazley [5]. Hoogendoorn prepared his flow pattern map using the mixture velocity and the gas percentage by volume as coordinates. He considered his map as a general one for gas-oil mixture flows. During his study of the effect of the liquid viscosity on the flow patterns, Hoogendoorn found that his map was also applicable to water-air mixture flows except for the wavy flow which occupied a larger region on the flow-pattern map. Considering that the transition lines were in fact transition zones with finite widths, Hoogendoorn concluded from his experiments, using different tube diameters, that the diameter had no effect on the transition lines between different flow regimes. Hoogendoorn also concluded that gas densities in the range fo 1.2 to 3.0 kg_m/m^3 and pipe relative roughness in the range of 0.0012 to 0.03 had no effect on the location of transition lines.

Based on adiabatic flow pattern data of other investigators, Baker [7] generated a generalized flow-pattern map in which the principal parameters were the gas and liquid mass velocities. To generalize the application of his map for any gas-liquid combinations, he introduced two correction factors, λ and ψ, which are functions of density, viscosity, and surface tension. These factors are given by:

$$\lambda = \sqrt{\frac{\rho_V/0.075}{\rho_\ell/62.3}}$$

$$\psi = \frac{73}{\sigma}\left[\mu_\ell\left(\frac{62.3}{\rho_\ell}\right)^2\right]^{1/3}$$

where ρ_v and ρ_ℓ are the vapor and liquid densities in lb_m/ft^3 respectively, μ_ℓ is the liquid viscosity in centi-poise, and σ is the liquid surface tension in dyne/cm.

Although Baker's map was developed for adiabatic horizontal flow, it has been applied with some success to adiabatic upflow. Goldmann [8] prepared flow pattern maps for adiabatic flow of steam-water mixtures, at different pressures, based on Baker's map by using the mass velocity and the vapor quality as coordinates.

Johnson and Abou-Sabe [9] presented their data on air-water flow patterns with heat transfer, and without phase change, on a map using air and water flow rates as coordinates.

In all references reviewed so far, no attempt was made by any of the investigators to establish, on a theoretical basis, the criteria that distinguish one flow pattern from another. Quandt [10] made the first attempt in this direction. His approach was based on the assumptions that:

1. The flow was adiabatic and both the gas, the liquid phases were flowing vertically upward.
2. The shearing stress acting on a fluid element existed only at the wall.

These assumptions limited the acting forces on a fluid element to three basic forces: axial pressure gradient force; gravitational force; and surface tension force. Quandt [10] assumed that each flow pattern was governed by a dominant force and a change in that dominant force meant a change in the flow pattern. Quandt's criteria for the existance of each flow pattern, together with the

procedure of constructing a flow regime map out of these criteria are discussed in detail and included in Chapter IV.

Diabatic Two-Phase Flow

During the past 20 years, the problem of diabatic two-phase flow received considerable attention by many investigators. Most of the references cited in this area were mainly concerned with the flow pattern and its effect on the heat transfer and pressure drop characteristics of forced convection boiling inside ducts of different geometries and orientations.

Berenson and Stone [11] studied the forced convection vaporization process of Refrigerant-113 inside a horizontal pyrex tube with high speed motion pictures. They observed flow regimes similar to those that occur in adiabatic flow. The data collected did not cover a wide range of operating conditions. As a result, no flow regime maps were constructed from their data.

Sheinin and Katarzhis [12] reported their data for evaporating water inside an electrically heated, inclined pipe having a 29.9 mm I.D. and 3.414 meters long. The pipe had a glass window made of optical quartz, and was installed at the downstream end of the pipe in the unheated section. Flow regimes were detected by electrical probes and also by visual observation. Tube inclination ranges of 5°26' to 9°43', and velocities up to 25 meters/second were covered by Sheinin and Katarzhis [12]. Also, their data were taken at three pressure levels, namely: 40, 70, and 120 atmospheres. Sheinin and Katarzhis constructed a set of flow regime maps using the mixture's velocity and the vapor volumetric ratio

as coordinates. Each of these maps corresponded to a certain pressure and tube inclination.

Hosler [13,14] photographed the flow patterns which existed during vertical flow of boiling water at high pressure in a narrow rectangular channel. He reconstructed Baker's [7] and Quandt's [10] maps together with a two-phase, adiabatic flow regime map using the total mass velocity and the quality as coordinates. When he plotted his results on these maps, Hosler [13,14] found that none of these maps correlated adequately his own results. As a result, he constructed a group of maps based on his results. Each of these maps corresponded to a certain working pressure. From these maps Hosler concluded that the increase in mass velocity tended to direct the transition lines towards lower qualities and that the inlet temperature and heat flux had no effect on the transition from slug to annular flow.

Staub and Zuber [15] used two identical vertical evaporators, one metallic for taking heat transfer data and the other glass for studying the flow regimes. Four high speed, 35 mm motion picture cameras were simultaneously used to study the flow patterns at four diferent glass sections. Observations and photographs identified four predominant flow regimes: bubbly, bubbly-slug, churn, and annular for evaporating Refrigerant-22 at reduced pressures of 0.12 and 0.22. Staub and Zuber used vapor and liquid superficial velocities as coordinates for their flow regime map and concluded that the local quality, total flow rate, and pressure are the most significant parameters in determining the flow pattern.

Hsu and Graham [16] reported the results of a visual and photographic study of the flow pattern of water, boiling inside vertical glass tubes of outside diameters 13 and 19 mms. Bubbly, slug, and slug-annular transition patterns were recorded by a high speed movie camera. Hsu and Graham concluded that flow pattern maps that were developed for two-phase adiabatic flow were not adequate for two-phase diabatic flow.

Vohr [17,18] conducted a photographic study of the flow patterns of water boiling inside a vertical rectangular channel at atmospheric pressure. His maximum mass flow rate and maximum water inlet velocity were 100,000 lb_m/hr. and 4 ft/sec., respectively. He observed bubbly, slug, and slug-annular flow patterns during the investigation.

Suo et al. [19] constructed a flow regime map for boiling water using the mass velocity and vapor quality as coordinates. On their flow pattern map, they reconstructed the transition lines between any two flow patterns by using different criteria developed by different authors for adiabatic two-phase flow. Suo et al. [19], based on their flow-pattern sutides of water boiling inside a vertical 0.4 in. I.D. tube, concluded that the adiabatic two-phase flow pattern criteria were not adequate for diabatic flow.

Zahn [20,21] studied the flow patterns of Refrigerant-22 evaporating inside horizontal tubes under pressures, temperatures, flow rates, and heat loading conditions similar to those occurring during the actual operation of a small air conditioning coil. The working pressure was 95 psia. The flow regimes were correlated by

constructing a map using the gas volumetric fraction and Froude number as coordinates. Zahn's data will be compared later with the data of this investigation.

Bergles and Suo [22] investigated the effect of different flow conditions on the flow patterns of boiling water inside vertical tubes. They observed that the increase in pressure or inlet temperature tended to shift all the transition lines towards higher qualities, while the increase in tube length tended to shift the transition lines towards lower qualities.

Griffith [23] studied the effect of pressure, tube diameter, and tube length on the quality at which transition from slug to annular flow is likely to occur. The liquid was pure water and the test section was an unheated glass tube mounted vertically downstream of an electrically heated metallic tube. The flow regimes were detected by two electrical probes mounted at both ends of the glass tube. From this study, Griffith found that the slug to annular transition occured at almost constant quality, whose value depended only on pressure. This was the case, provided that the condition $V^2\rho_v/gD\rho_\ell > 2$ was satisfied. V, ρ_v, g, D, and ρ_ℓ are superficial vapor velocity, vapor density, gravitational acceleration, tube diameter, and liquid density, respectively.

From the above literature survey, it can be emphasized that:

1. Flow pattern maps that were developed for two-phase adiabatic flow were not adequate for identifying the flow pattern of diabatic two-phase flow.
2. All diabatic flow-pattern studies were concerned with boiling.

3. No flow-pattern studies during condensation could be found. It is the objective of this investigation to perform such a study.

CHAPTER III

EXPERIMENTAL INVESTIGATION

The objectives of this experimental investigation are:

1. To visually and photographically study the flow patterns, during forced convection condensation inside a 0.5 in. I.D. horizontal tube, under different flow conditions. The condensing fluid to be used is Refrigerant-12.
2. To construct flow-pattern maps for condensation and to compare them with the flow-pattern maps available in literature.

Experimental Facility

The experimental test facility that was used by Abis [24] was modified to permit taking the required data of the present investigation. The test facility contained the essential components of a Refrigerant-12 vapor compression refrigeration system. Figure 4 shows a schematic diagram of the Refrigerant-12 flow circuit, and Plate I shows a photographic view of the test facility. The main components of the system were:

1. 2-h.p. Copeland compressor
2. Main test condenser
3. Vapor-liquid separator
4. After condenser
5. Liquid receiver
6. Water chiller (evaporator)
7. Hand operated expansion valve

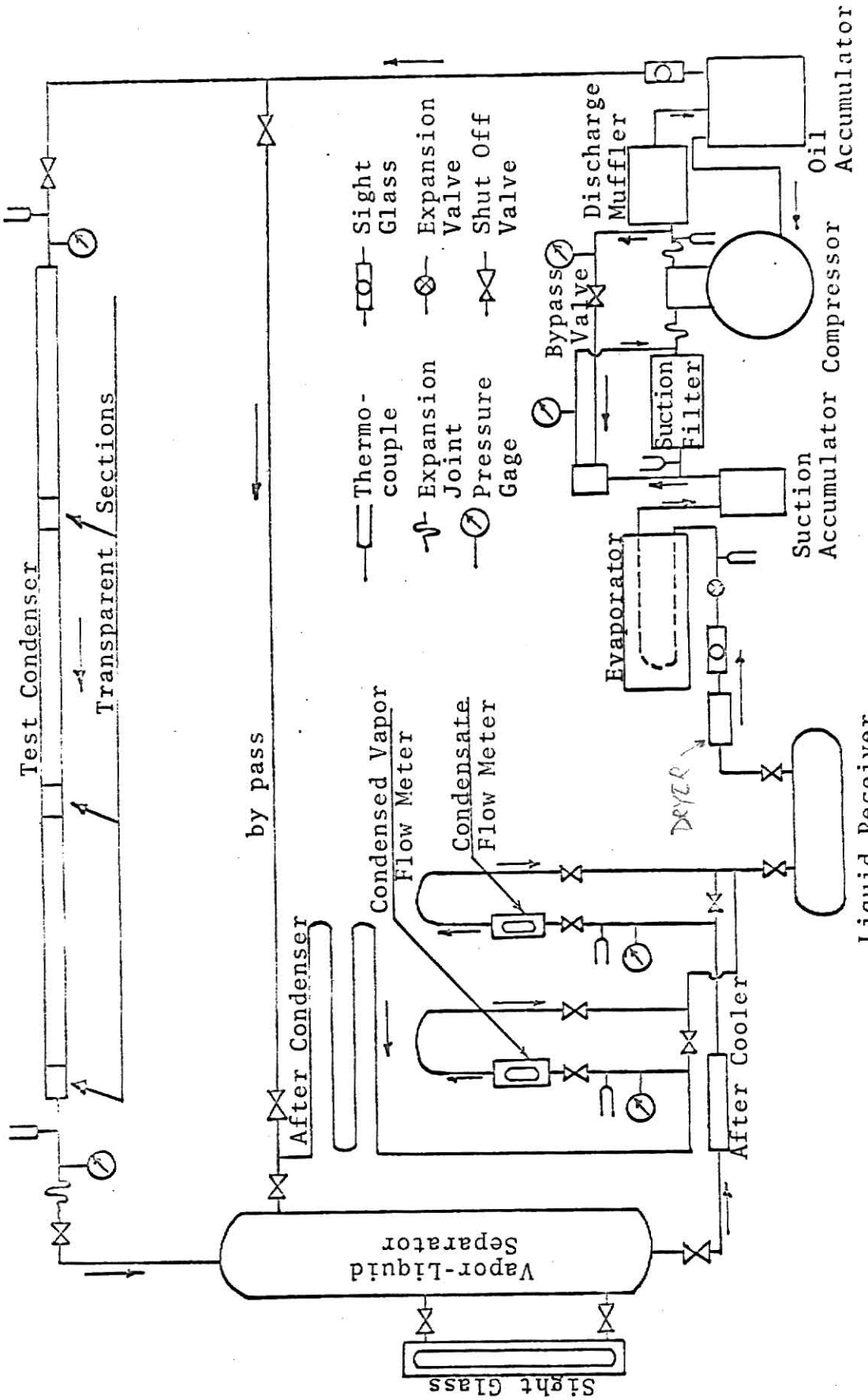

Fig. 4. A Schematic Diagram for the Refrigerant-12 Circuit.

EXPLANATION OF PLATE I

Photographic view showing the experimental facility used in this investigation. Numbers on the photograph are to identify the following components:

1. Test condenser
2. Vapor-liquid separator
3. After-condenser
4. Condensed vapor flow meter
5. Condensate flow meter
6. Cooling water flow meter
7. Liquid accumulator
8. Evaporator
9. Expansion valve
10. Compressor
11. Multi-channel precision potentiometer

PLATE I

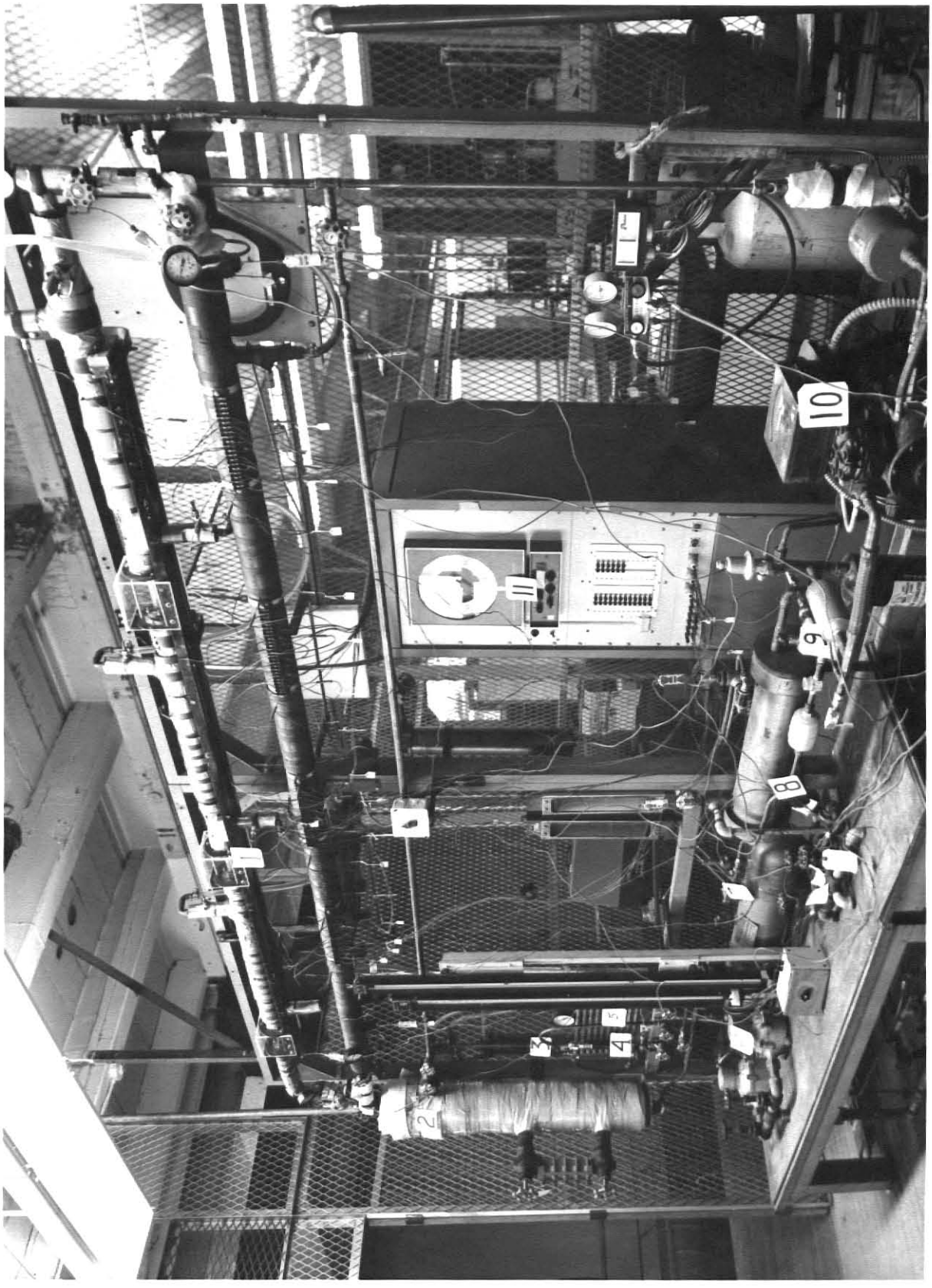

The auxillary components were:

1. Refrigerant drier-filter
2. Suction accumulator
3. Suction filter
4. Oil separator
5. Discharge muffler
6. Low and high pressure safety switch
7. Coolant filters
8. Coolant circulating pump

The instrumentation of the test facility included:

1. Integrating type flow meter for coolant flow measurements
2. Refrigerant flow meters of the variable area type
3. Multi-channel indicating potentiometer to measure the thermocouples e.m.f. output

Figure 5 shows the flow diagram of the cooling water circuit. The cooling water circuit was designed to permit the control of the temperature of the cooling water to the test condenser. This could be achieved by mixing the return water from the after-condenser, the test condenser, and the water chiller with the city water (in a mixing tank) before the water was recirculated by the pump. By this method, it was possible to control the condensing pressure of the refrigerant, in the test section, as well as the mass flow rate of the refrigerant.

Test Condenser and Instrumentation

Figure 6-a shows a schematic diagram of the experimental test condenser that was designed and constructed essentially for this

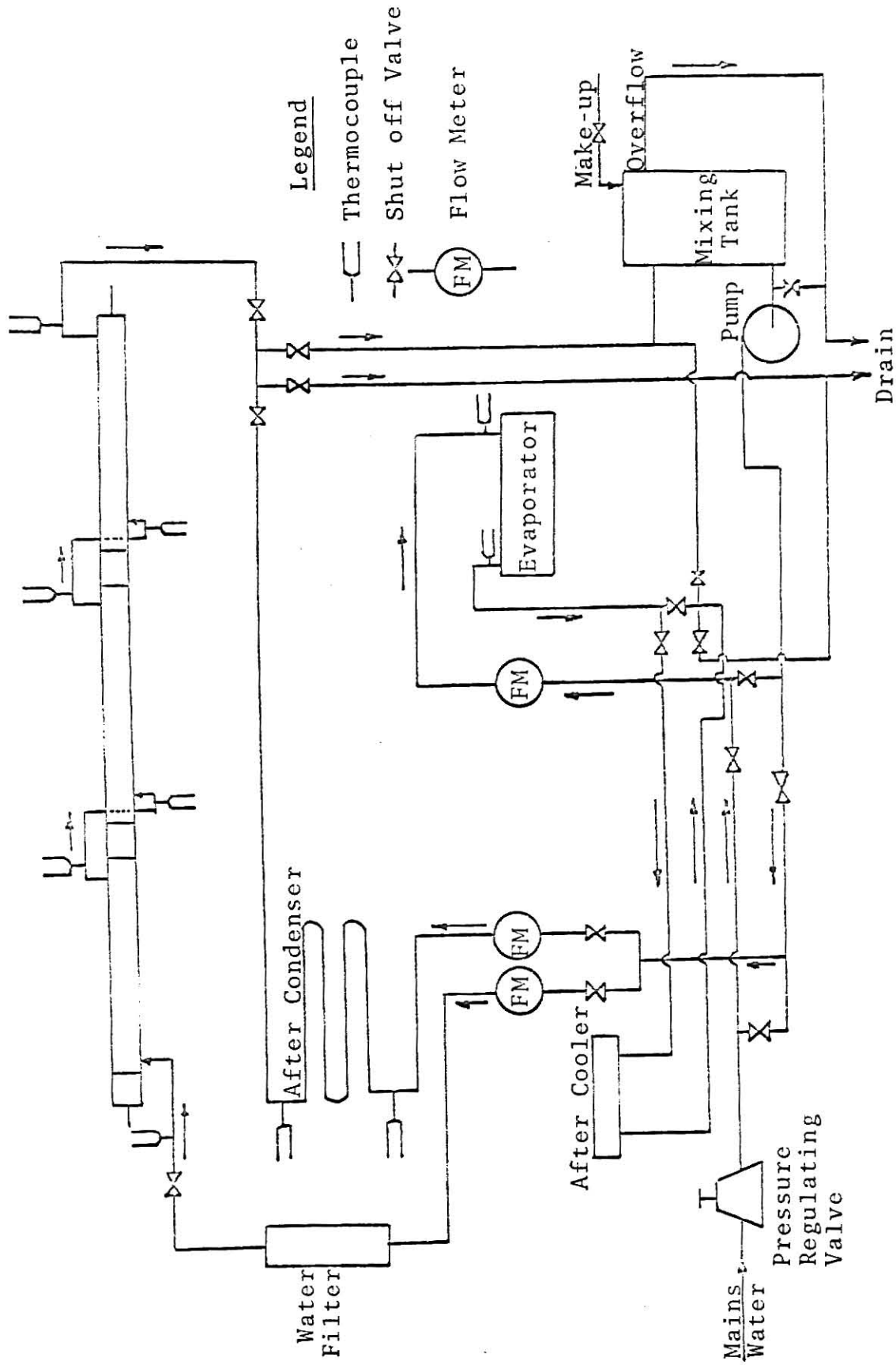

Fig. 5. A Schematic Diagram for the Cooling Water Circuit.

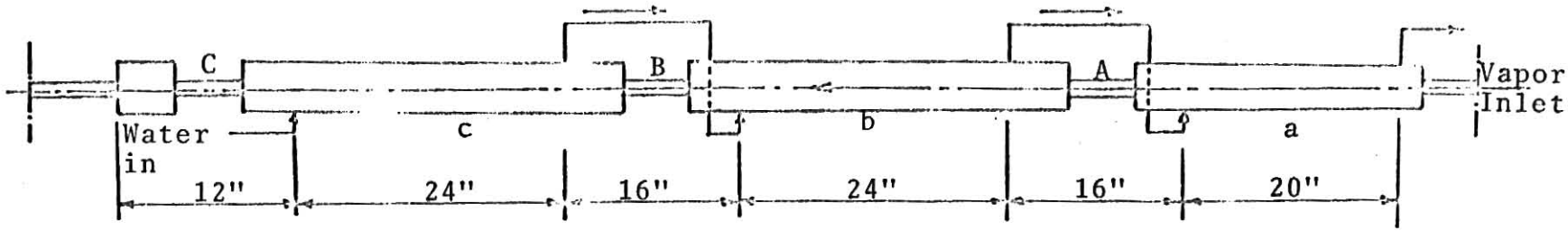

Fig. 6-a. A Schematic Diagram for the Test Condenser.

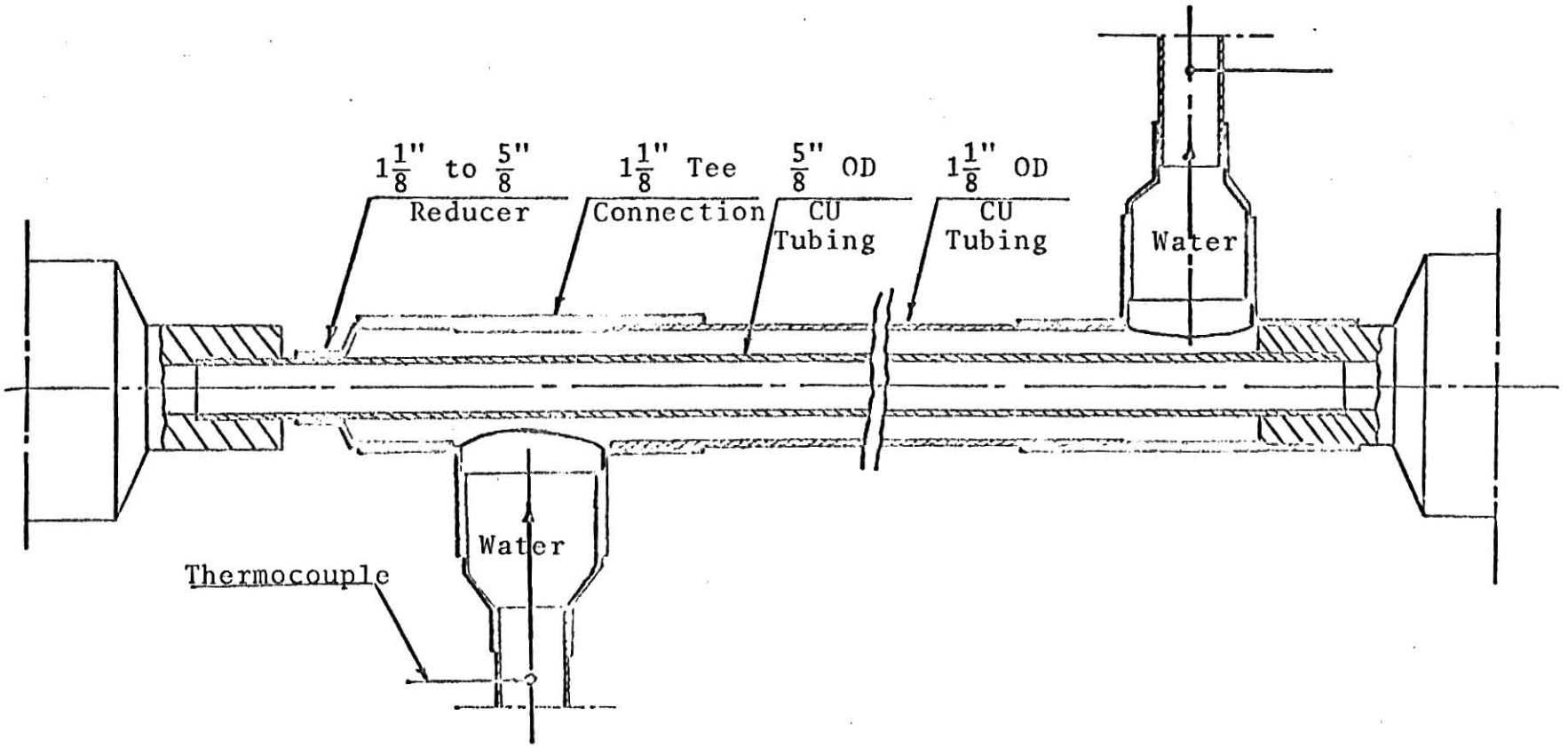

Fig. 6-b. Construction Details of Condenser Sections a, b, or c.

investigation. Basically, it consisted of three separate double pipes, counter flow condensers labeled a, b, and c in Fig. 6-a. Each of these condensers was constructed separately. The inner tube of each condenser was a copper tube having 1/2 in. I.D. and 5/8 in. O.D. The outer jacket was also a copper tube having a 1 in. I.D. and 1-1/8 ins. O.D. Condensers a, b, and c had overall lengths (from water inlet to water outlet) of 20, 24, and 24 ins., respectively. Figure 6-b shows the construction details of one of these condensers. Condensers a, b, and c were joined together by three transparent glass tubes, labeled A, B, and C in Fig. 6-a, to form the entire test condenser. Plate II shows a photographic view of the entire test condenser. Each glass tube had a 1/2 in. I.D. and 3/4 in. O.D. and an overall length of 8-1/2 ins. The cooling water entered the cooling jacket of condenser c in a counter flow direction to the refrigerant flow, then entered condensers b and a successively after leaving condenser c. Figure 7 shows the construction details of the transparent sections. Each transparent section was made of standard clear, high pressure tubular gage glass, and was fitted between two adjacent condensers by two stuffing boxes. Three 3/8 in. diameter tie rods were used to secure together the two stuffing boxes at the ends of each transparent section to prevent leakage.

Each of the three visual sections was leak-proof tested individually, for 24 hours, under pressures as high as 200 psig. Such a pressure was higher than any pressure encountered during the experiments. They were also leak-proof tested under vacuum as low as 1000 microns. The three condensers a, b, and c and the three

EXPLANATION OF PLATE II

Photographic view showing the test condenser. Numbers on the photograph are to identify the following components:

1. Condensing unit a
2. Visual section A
3. Condensing unit b
4. Visual section B
5. Condensing unit c
6. Visual section C

PLATE II

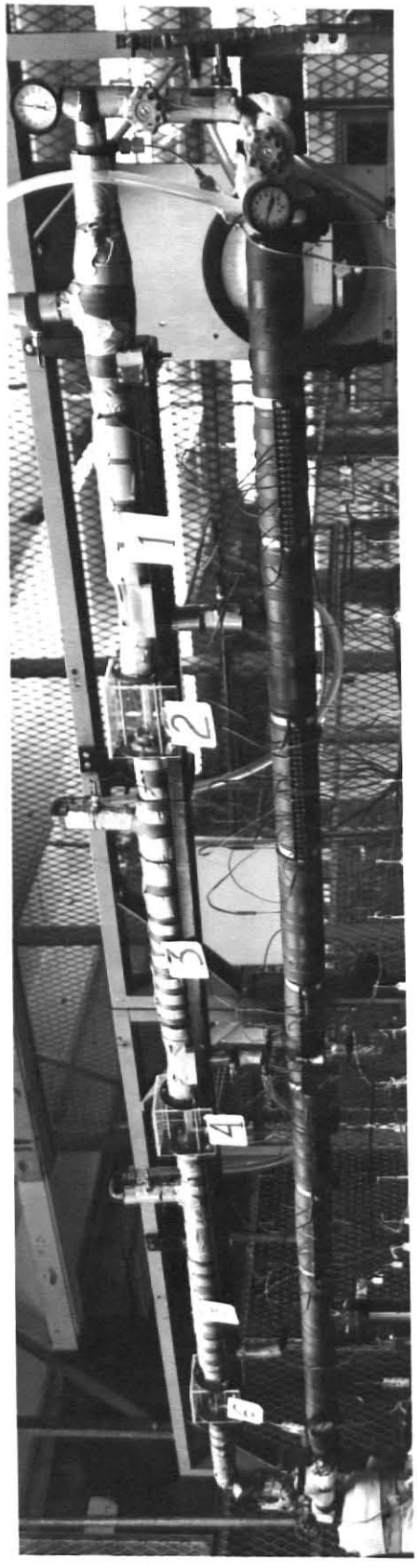

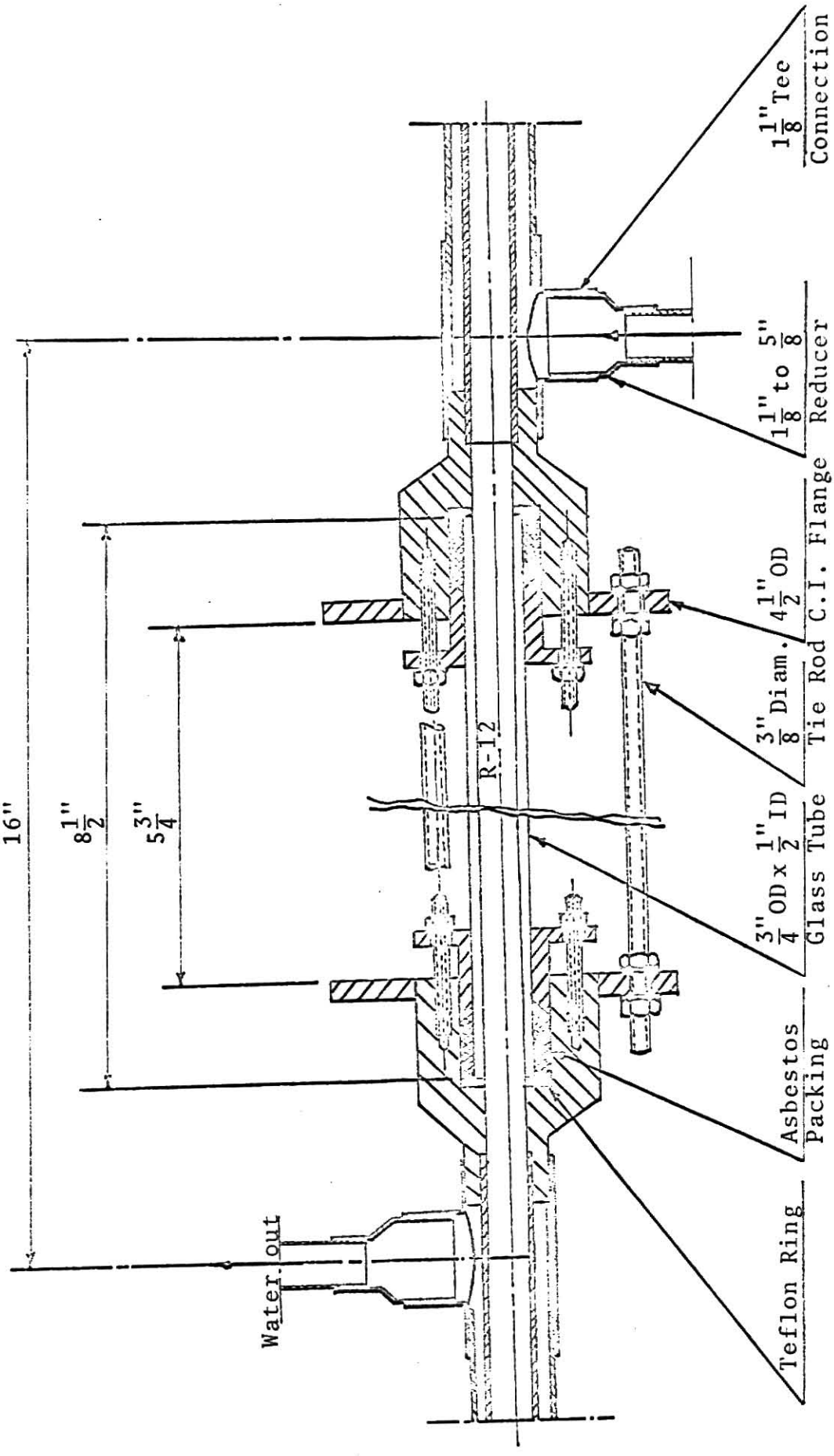

Fig. 7. Construction Details of the Transparent Section.

transparent sections A, B, and C were mounted individually on supports. While being supported in a horizontal position, they were drawn together and then welded. Before welding, all condensers and transparent sections were checked individually by a liquid level, to make sure that they were all mounted horizontally and coaxially aligned. An expansion joint was added at one side of the condenser to accomodate any expansion, due to heating, during operation. With the entire condenser assembled, it was checked again for leaks under pressurized and evacuated conditions. The entire system was then evacuated down to 1000 microns and charged with refrigerant-12.

Each of the condenser sections a, b, or c was instrumented to measure the inlet and outlet temperatures of the cooling water through each condenser. The inlet and outlet temperatures of the refrigerant to the entire test condenser were also measured. All temperatures were measured by copper-constanan thermocouples of 24 B and S gage wire. Inlet and outlet pressures of the refrigerant were also measured. The cooling water flow rate was measured by the flow meter mounted on the cooling water circuit. All thermocouples were calibrated against the temperatures of boiling water and melting ice. Their e.m.f. output was measured by Honeywell Electronic-18 multi-channel potentiometer. The liquid refrigerant flow rate from the liquid-vapor separator represented the amount of refrigerant condensed in the test condenser. Its flow rate was measured by a Fisher-Porter variable area type flowmeter. The vapor from the separator which was condensed in the

after condenser was also measured by a second Fisher-Porter variable area type flow meter. The combined flow rate readings of the two flow meters represented the total mass flow rate of the refrigerant through the test condenser. Condenser sections a, b, and c were insulated with 2-1/2 ins. thick rubber insulation. The liquid-vapor separator was also insulated with 3/4 in. thick fiber glass insulation.

Visual and Photographic Study of Flow Pattern

In this investigation 42 runs were performed covering a wide range of condensing pressures, mass velocities, and included all possible flow patterns. During each run, the flow pattern during condensation could be visually observed and identified in any of the transparent sections A, B, and C, which are shown in Fig. 6-a. For economical reasons, no attempt was made to take high speed motion pictures for each run at each transparent section of the test condenser. However, one high speed motion picture was taken for each of the nine flow patterns that could be identified. It was mainly relied on visual observation to identify the flow pattern, at any of the transparent sections, during all the runs.

Photographic Equipment

Figure 8 shows a schematic diagram of the photographic equipment used in this investigation. It includes a high speed motion picture camera, a control or "goose" unit, and lighting equipment.

The camera was a Fastax WF3 type camera which used 100-ft reels of 16 mm film. It had a maximum speed of 8000 frames/sec.

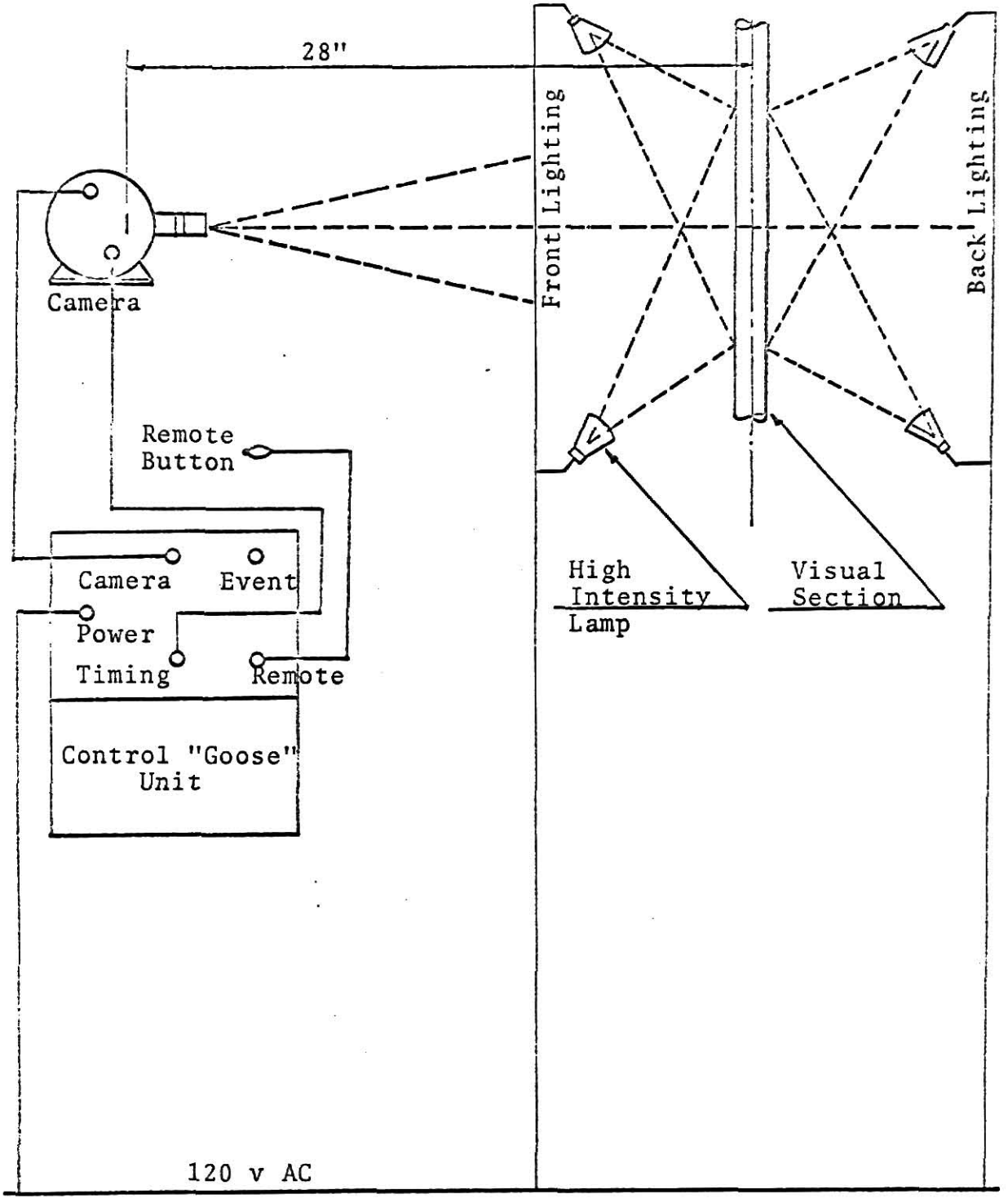

Fig. 8. Schematic Diagram for the Photographic Equipment

Different film speeds could be obtained by controlling the voltage applied to the motors of the camera through the "goose" unit. The speed of the camera was registered on the film edge by a timing device which consisted of a neon glow lamp enclosed in the camera housing. The lamp was energized by A-C current and the light emitted from both plates of the lamp was focused on the edge of the film. Lamp operations resulted in timing marks which appeared as a 2.5 mm wide black line along one edge of the developed film outside the picture area. When the timing light was connected directly to a 60 cycle A-C power supply, which was the case during the whole experimental investigation, and there were 33 pictures between two successive timing marks, the camera's speed was 4000 frames/second. Eastman 4-x, black and white negative films (type 7224) were used. The lighting sources used for illumination were two 375-watt lamps placed on the camera side of the transparent section and two 125-watt lamps placed behind the test section. All light sources were placed at an enclined angle as shown in Fig. 8. The decision on this type of lighting arrangement was reached after a number of trial runs until the best motion pictures could be produced. Plate III shows a photographic view of the photographic equipment.

Test Procedure

Before the compressor was started, the cooling water mixing tank was filled to the overflow level, and city water was allowed to flow into the tank continuously. The compressor and the circulating water pump were put into operation simultaneously after

EXPLANATION OF PLATE III

Photographic view of the high speed motion picture camera and the supporting equipment.

PLATE III

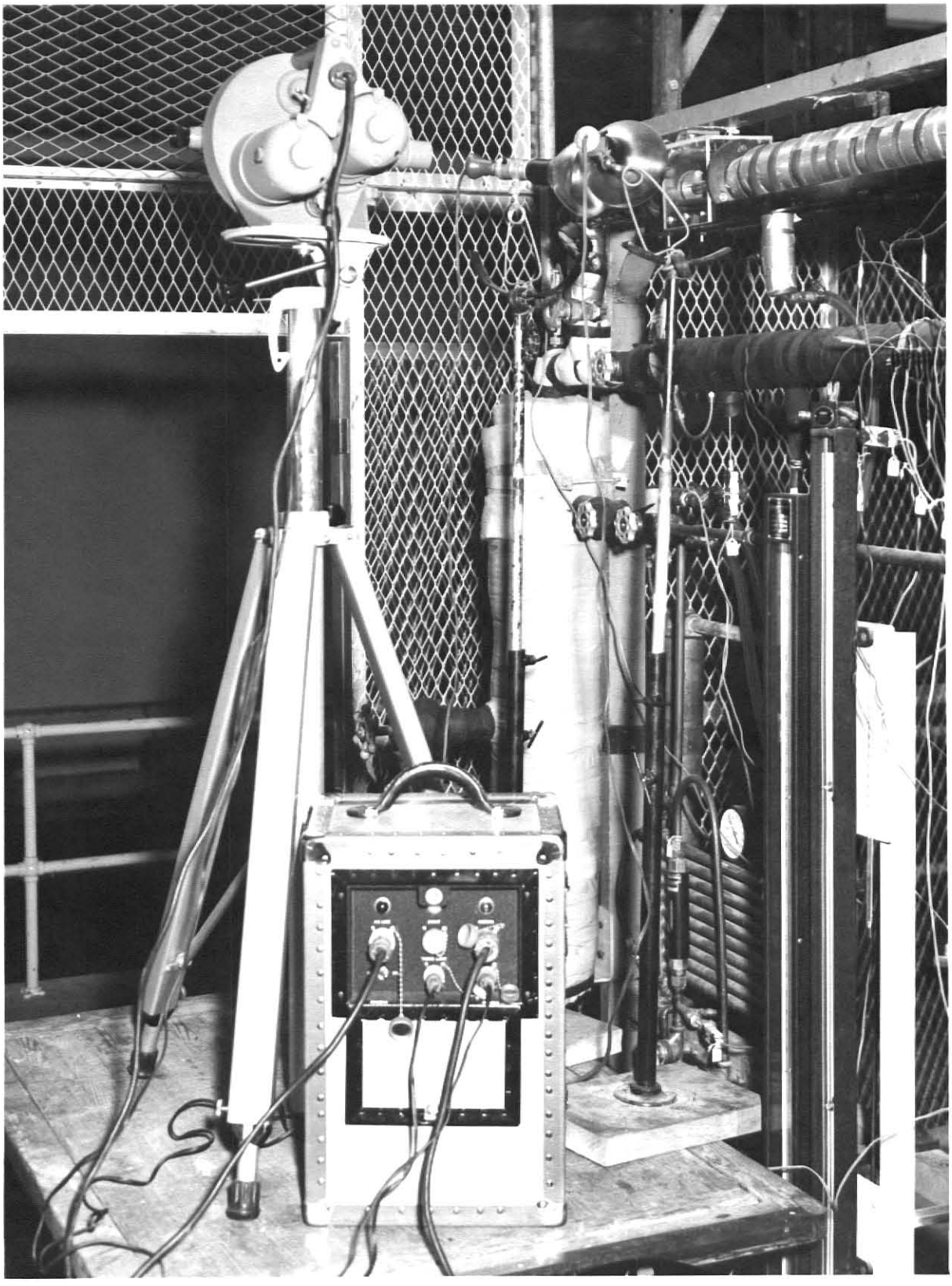

equalizing the pressure of both compressor sides through the by-pass valve. The system was allowed to run while necessary adjustments were being made to get the required operating conditions such as refrigerant flow rate and condensing pressure. The adjustments of the cooling water flow rates to the test condenser and after condenser, the opening of the hand-operated expansion valve, the opening of the compressor by-pass valve, and the water flow rate to the evaporator were used to change the refrigerant mass flow rate and condensing pressure from one run to the other. Steady state conditions were established when the readings of all pressure and temperatures measuring instruments and the liquid refrigerant level in the vapor-liquid separator remained unchanged for an extended period of time. The liquid level in the separator could be determined by the sight glass attached to the separator and could be controlled by the opening of the upstream valves of the refrigerant flow meters. Steady state conditions could be reached in any run within two hours, however, the system was allowed to run for a period of three hours before any readings and visual or photographic data were recorded. During each run, the following measurements were taken:

1. Water flow rates to the test condenser and after condenser
2. Refrigerant's inlet and exit gage pressures
3. Refrigerant's inlet and exit temperatures in millivolts
4. Inlet and exit coolant temperatures, of the test condenser sections a, b, and c in millivolts. There were six readings in each run

5. Flow rates of the two refrigerant flow meters in gallons/minute

In addition to the above readings, the ambient temperature and the barometric pressure were recorded during each run. Also, for each run, the flow patterns were observed and recorded at each of the transparent sections. Nine flow patterns were identified during this investigation. These flow patterns were: spray, spray-annular, annular, semiannular, annular-wavy, semiannular-wavy, wavy, slug, and plug flows. These flow patterns will be discussed in a later section.

As it was mentioned earlier in this section, high speed motion pictures were taken for certain runs covering all the nine different flow patterns that could be identified visually in this investigation. For the specific runs that were chosen for taking the motion pictures, and while waiting for the system to reach the steady state condition, the camera was loaded, focused, and the lighting and the lens aperature were adjusted. When steady state conditions were established, the camera was started and the flow pattern of interest in that particular run was photographed.

CHAPTER IV

EXPERIMENTAL RESULTS AND DISCUSSION

Experimental Results

The range of conditions covered in this investigation can be summarized as follows:

1. Condensation pressure, 90-127 psia
2. Condenser tube diameter, 0.5 in.
3. Condenser over-all length, 100 ins.
4. Refrigerant mass velocity, 18,860-223,600 $lb_m/hr.ft^2$
5. Inlet superheat, 53-126°F. (25.72 - 30.49 lbm/hr.)
6. Vapor exit quality, 0.00-0.95 (0.429 - 0.508 lbm/min.)
7. Coolant flow rate, 410-2,698 $lb_m/hr.$
8. Average heat removal rate from condensing Refrigerant-12, based on condenser's inner diameter, 2,500-16,600 Btu/hr. ft^2

The transparent sections were located at 20, 60, and 100 ins. downstream from the vapor inlet as shown in Fig. 6-a. Table B-1 of Appendix B includes a summary of the operating conditions of the forty-two runs covered by this investigation. The values of the pressure listed in this table represent the average pressure between inlet and outlet conditions. The temperatures listed are the saturation temperatures corresponding to the average condensation pressures. Refrigerant's mass flow rate was estimated from the sum of the two flow meters located after the liquid separator and the after condenser. Refrigerant's mass velocity was based

on the total cross-sectional area of the condenser's tube inner diameter. The heat rate gained by the cooling water was calculated from the water flow rate and the overall temperature difference between inlet and outlet of each of the condensing sections a, b, and c. The heat rate lost by the condensing fluid was estimated from the total mass flow rate of the refrigerant and its overall enthalpy change between inlet and outlet. The heat balance error was calculated from the ratio of the difference between the heat rates of the coolant and the refrigerant, to the heat rate of the coolant. It is to be noticed that the heat balance error was within ±13% in almost all runs except in run 4 where the heat balance error was 52%. This may be attributed to an error in the refrigerant flow rate.

Table B-2 summarizes the thermophysical properties of Refrigerant-12 corresponding to each run. They are based on the saturation temperatures corresponding to the average condensation pressures. All properties were taken from the ASHRAE Handbook of Fundamentals [25]. In the same table, Baker's [7] correction factors λ and ψ, which are functions of the condensing fluid properties, are also listed. Reference will be made later to these two parameters.

Tables B-3 and B-4 list the significant flow parameters that were used in constructing the different flow pattern maps that will be discussed later in this chapter. These parameters were calculated for each of the flow conditions in the transparent sections A, B, and C. A sample of the calculations, based on the

data of run 16, is included in Appendix C. The last columns of Tables B-3 and B-4 list the flow patterns observed during all the runs at the different transparent sections. Nine different flow patterns were observed. The descriptions and characteristics on which basis the flow pattern was visually identified were:

1. Plug Flow: This flow was formed of a continuous liquid phase with large plugs of vapor that appeared intermittently at the top of the tube.
2. Slug Flow: This flow was formed of liquid flowing in the lower part of the tube and vapor flowing at a relatively higher speed on top of it. The relative speed between liquid and vapor was high enough to form frequent slugs of liquid which wetted the top of the tube.
3. Wavy Flow: In this flow pattern, the two phases were separated, with the liquid flowing at the bottom of the tube. The difference in velocity between liquid and vapor caused the interface to be wavy.
4. Annular Flow: A layer of liquid covered the entire tube wall while the core was filled with vapor which usually contained some liquid droplets.
5. Semiannular Flow: The flow had the same appearance as the annular flow, but the amount of condensed liquid was not enough to cover the entire tube periphery. Part of the upper half of the tube appeared dry.
6. Annular-Wavy Flow: The flow had an annular appearance with the top part of the tube becoming occasionally dry

and the liquid thickness at the tube bottom was relatively bigger.

7. Semiannular-Wavy Flow: The flow had the semiannular appearance except that the liquid thickness at the tube bottom was relatively bigger.
8. Spray Flow: No liquid layer was apparent around the tube, and almost all the liquid was entrained within the vapor as a mist.
9. Spray-Annular Flow: The layer of liquid that existed in the annular flow around the tube became very thin and was continuously swept and entrained within the vapor as a mist.

Figure 9 illustrates the above patterns as they were observed during the experimental runs. Six of these nine flow patterns can be considered as major ones while the others can be considered as transitions between these major patterns. The major patterns are the plug, slug, wavy, semiannular, annular, and spray flows. It was possible to identify the nine flow patterns by visual observations. However, after taking high speed movie pictures for these flow patterns, only the major patterns could be identified. The remaining three looked exactly alike. The high speed movie pictures of the major flow patterns were included in a 6-minute motion picture film and have been filed at the Kansas State University Department of Mechanical Engineering library. Figure 10 includes six photographic pictures of the major flow patterns. These pictures were reproduced from the motion picture film.

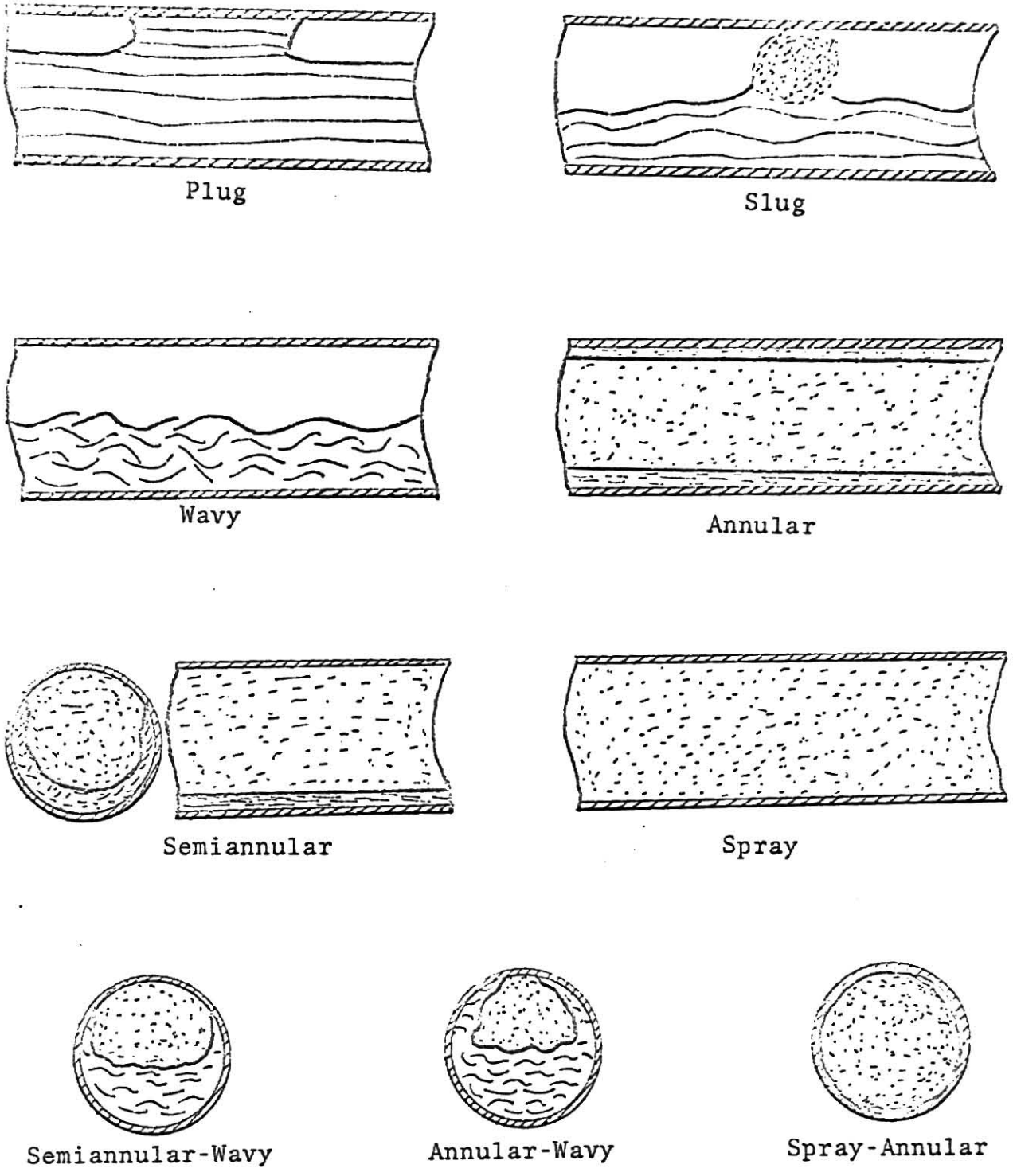

Fig. 9. A Schematic View for the Observed Flow Patterns.

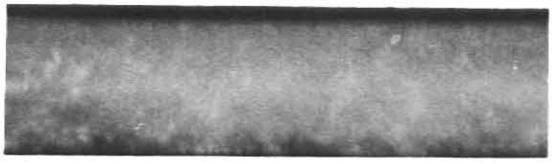

Spray Flow
Run No. 42
Visual Section A

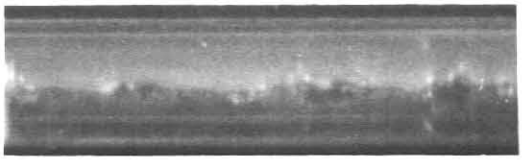

Wavy Flow
Run No. 40
Visual Section C

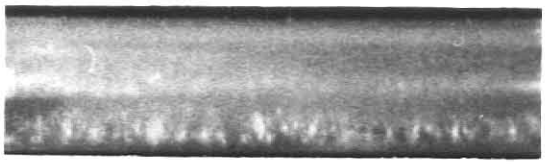

Semiannular Flow
Run No. 24
Visual Section B

Slug Flow
Run No. 26
Visual Section C

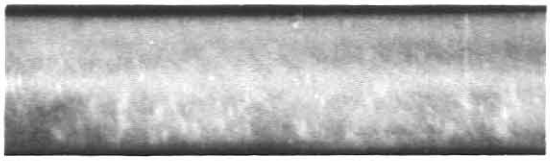

Annular Flow
Run No. 38
Visual Section C

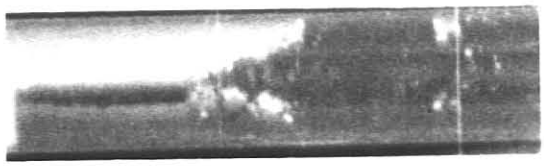

Plug Flow
Run No. 13
Visual Section C

Fig. 10. Photographic Views for the Major Flow Patterns.

Data Representation

It has been pointed out earlier, in the literature survey, that there is generally no standard way for presenting the data of two-phase flow-pattern studies. Baker's [7] flow-pattern map was one of the earliest maps used, and is still being used, in adiabatic two-phase, two-component (gas and liquid) flow. Flow pattern parameters, different from those used by Baker, were used by different investigators [12,14,15,20,21,22] in constructing flow pattern maps for diabatic two-phase flow, specifically for boiling. No flow pattern maps are available, at the present time, for condensation. The attempt was made in this section, to present the data of the present investigation by constructing several flow pattern maps using flow pattern parameters that were used by other investigators. Also comparison between flow pattern maps, developed for condensation, and those that were developed by other investigators, for adiabatic and diabatic two-phase flow, was made.

Figures 11-a and 11-b show the data of the 42 runs plotted on maps using the same parameters used by Zahn [20,21], namely: Froude number and the gas volumetric ratio. Frounde number N_{FR}, is defined by

$$N_{FR} = \frac{(V_{vs} + V_{\ell s})^2}{gD}$$

and, the gas volumetric ratio R, is defined by

$$R = \frac{Q_v}{Q_\ell + Q_v} = \frac{(V_{vs}/V_{v\ell})}{(V_{vs}/V_{\ell s}) + 1} \quad *$$

---

*See Appendix A for the definition of symbols.

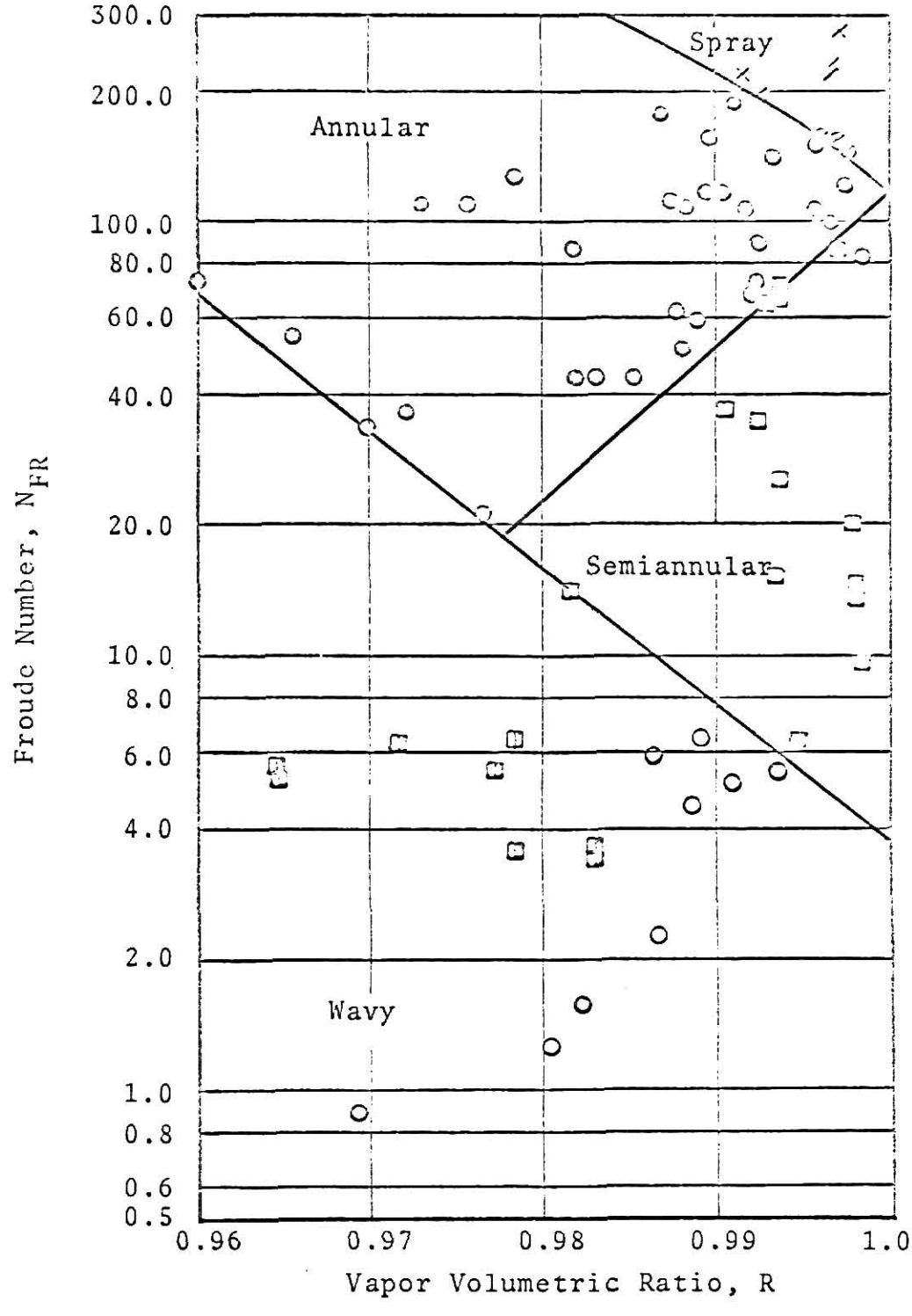

Fig. 11-a. Flow Pattern Map Based on Froude Number and Vapor Volumetric Ratio.

Spray	×	Semiannular-wavy	⊏
Spray-annular	⊗	Annular-wavy	◡
Annular	○	Wavy	○
Semiannular	⊏	Slug	△
		Plug	▲

These same symbols will be used in the remainder of the figures.

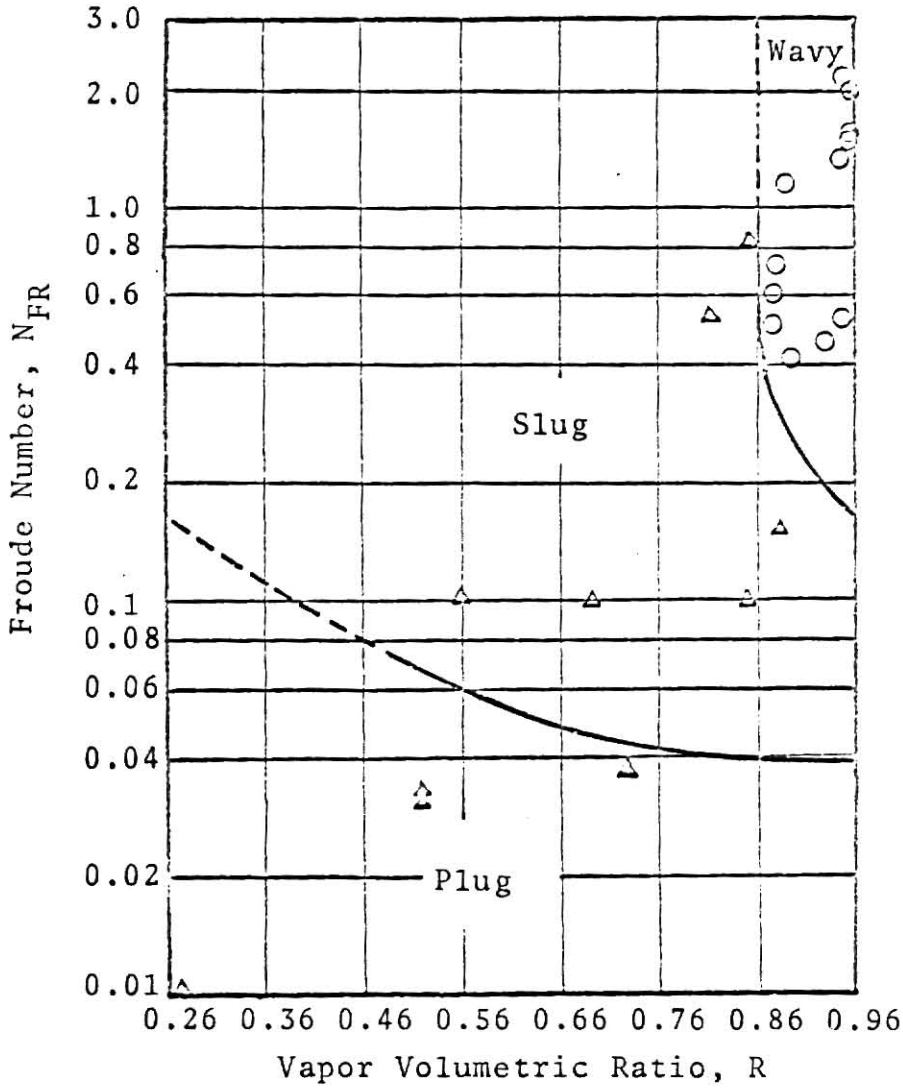

Fig. 11-b. Flow Pattern Map Based on Froude Number and Vapor Volumetric Ratio.

In his visual study of two-phase flow of Refrigerant-22 evaporating inside a horizontal tube, Zahn [20,21] pointed out the fact that these two parameters have the advantage, over Baker's [7] parameters, of being dimensionless. In addition, both parameters are compatible with the physical interpretations of the boundaries between the different flow regimes.

It is to be pointed out that the results were deliberately plotted on two different plots, namely Figs. 11-a and 11-b. The first includes the spray, annular, semiannular, and wavy patterns. The second includes the wavy, plug, and slug patterns. Both plots differ in the scale used for the gas volumetric ratio. Had all the results been plotted on a single plot, the results would have crowded at the extreme ends of the abscissa. On each of the two figures the boundaries between the main flow patterns (plug, slug, wavy, annular, semiannular, and spray) were arbitrarily drawn. It is to be emphasized that, in actuality, there is no sharp boundary between any two flow patterns, but there is, rather, a transition zone. A great deal of personal judgment was involved in drawing these boundaries. It is also to be noticed that there is a wide transition zone between the annular or semiannular and the wavy flow. These are the annular-wavy and semiannular-wavy regimes. However, the transition zone between wavy and slug or slug and plug is not as wide. The boundary lines between wavy-slug and slug-plug flows were drawn as solid lines in the regions where data were available and were arbitrarily extended as dotted lines in the region where data points were not available.

The results of Figs. 11-a and 11-b seem to indicate that the flow pattern is a function of Froude number and gas volumetric ratio. It is to be recalled that Froude number is a measure of the ratio of inertia forces to gravitational forces and that the gas volumetric ratio is a measure of the ratio of the vapor superficial velocity to the liquid superficial velocity. Annular, semiannular, and spray flows seem to occur at relatively high Froude numbers ($N_{FR} > 10$), and high vapor volumetric ratios ($R > 0.96$). In these types of patterns, the inertia forces dominate the gravitational forces. In addition, the superficial vapor velocity is high enough, compared to the superficial liquid velocity, to sustain a liquid film of a finite thickness as in the case of annular or semiannular flow. Beyond a certain vapor superficial velocity, the liquid film breaks into a uniform spray without any liquid film being evident.

The transition between the spray and annular flows can be related to the dimensionless parameter known as Weber number. Weber number is defined by:

$$N_{WE} = \frac{(V_{vs} + V_{\ell s})^2 \rho_{av} D}{g_c \sigma}$$

It represents the ratio of inertia forces to surface forces. The annular flow pattern is characterized by the presence of a stable liquid film around the tube. The liquid film remains stable as long as the surface forces are in equilibrium with inertia forces. Data in Table B-3 indicate that the transition between annular and spray flows occurred at a critical Weber number having a value of

$(N_{WE})_{critical}$ = 2,300-2,400. Annular flow has a lower Weber number, while spray flow has higher values than the critical Weber number.

Slug, plug, and wavy flow seem to occur at lower Froude numbers (N_{FR} < 10). The results indicate that these flow patterns occurred in the following ranges of Froude numbers and vapor volumetric ratios:

wavy flow: $0.4 < N_{FR} < 7$

$0.86 < R < 0.993$

slug flow: $0.1 < N_{FR} < 0.8$

$0.56 < R < 0.86$

plug flow: $N_{FR} < 0.1$

$R < 0.76$

It is the combined effect of these two parameters that determines the flow pattern. In all three patterns (slug, plug, and wavy), the gravitational forces are significant and cause the liquid to flow at the bottom of the tube and the vapor at the top.

Figure 12 shows a flow pattern map reproduced from the results of Figs. 11-a and 11-b. No data points are shown in this figure. Only the transition lines between the spray, annular, semiannular, and wavy flows are shown in solid lines. In the same figure, the transition lines between the different flow regimes, that were developed by Zahn [20,21] from his visual study of flow patterns of Refrigerant-22 evaporating in horizontal tubes, were drawn as dotted lines. Several remarks about the results of Fig. 12 are in order. First, at the same value of vapor volumetric ratio,

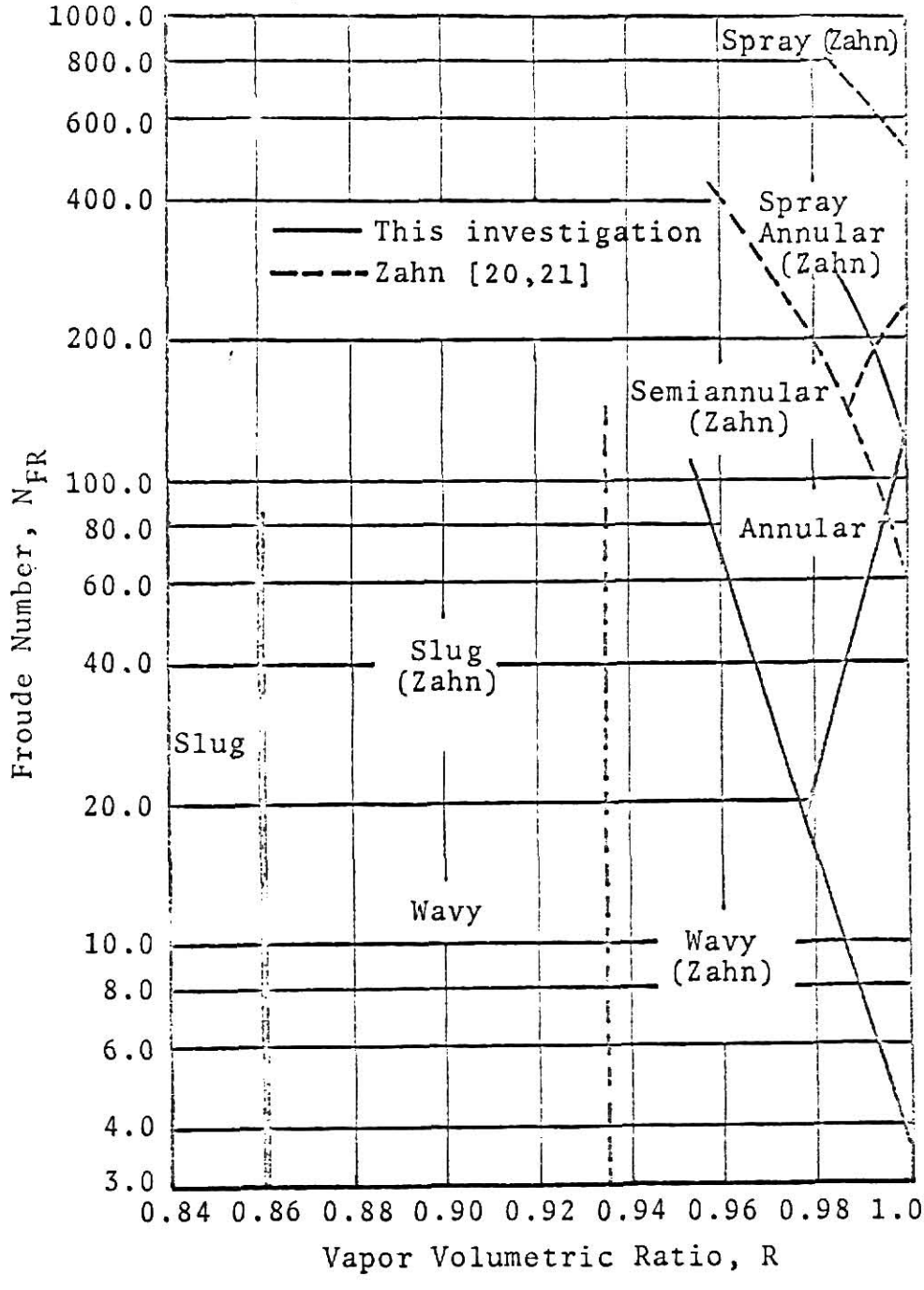

Fig. 12. Comparison Between the Flow Pattern Map Developed by Zahn [20,21] and the Map Developed in This Investigation.

Zahn's [20,21] transition lines occur at slightly higher values of Froude number. Second, at the same value of Froude number, Zahn's [20,21] transition lines occur at slightly higher gas volumetric ratios. Considering the fact that these transition lines are actually transition zones, it can be said that the agreement between Zahn's results and the results of the present investigation is fair.

Figure 13 shows a flow pattern map constructed from the results of the present investigation using Baker's [7] parameters. These parameters were calculated for all the runs and are given in Table B-3 of Appendix B. The transition lines between any two flow patterns were arbitrarily drawn. To compare the flow pattern map of Fig. 13 with Baker's [7] flow pattern map, all the main different flow pattern areas of Fig. 13 were transferred to cross-hatched areas on Baker's [7] map of Fig. 14. For the sake of comparison, Fig. 15 was reproduced from reference [20] to compare the flow regime areas of evaporation to Baker's [7] flow regime areas. Figures 14 and 15 show that the two-phase flow pattern map developed by Baker for adiabatic flow, is not adequate for predicting the flow pattern for diabatic flow (evaporation and condensation). Also, it is to be noticed that certain flow patterns during condensation or evaporation, occupy approximately the same areas on Baker's map. These are the spray, annular, semiannular, and wavy patterns.

Some flow pattern maps were developed by different investigators for adiabatic [1], and diabatic [15] two-phase flow, using

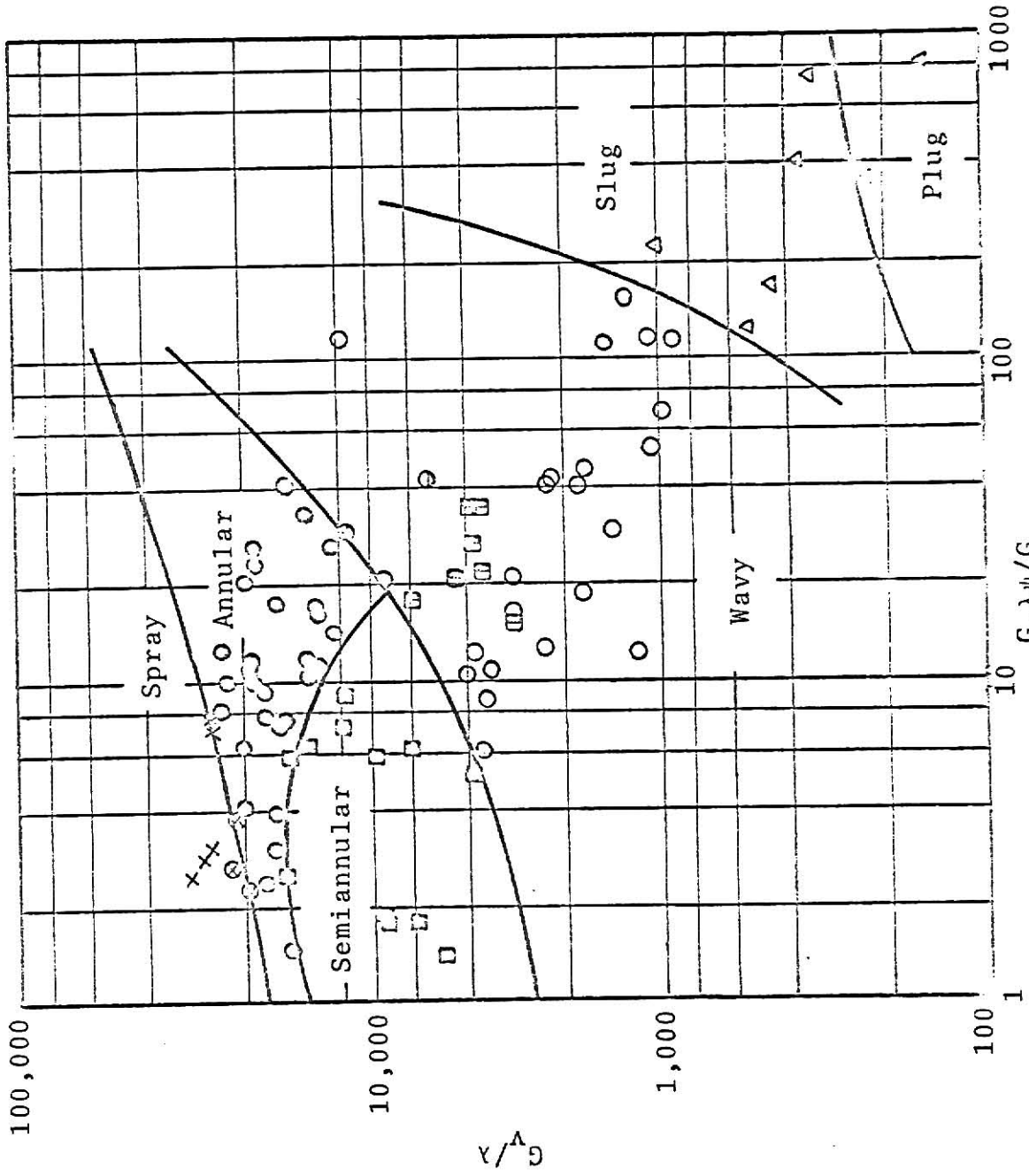

Fig. 13. Flow Regime Map Using Baker's [7] Coordinates.

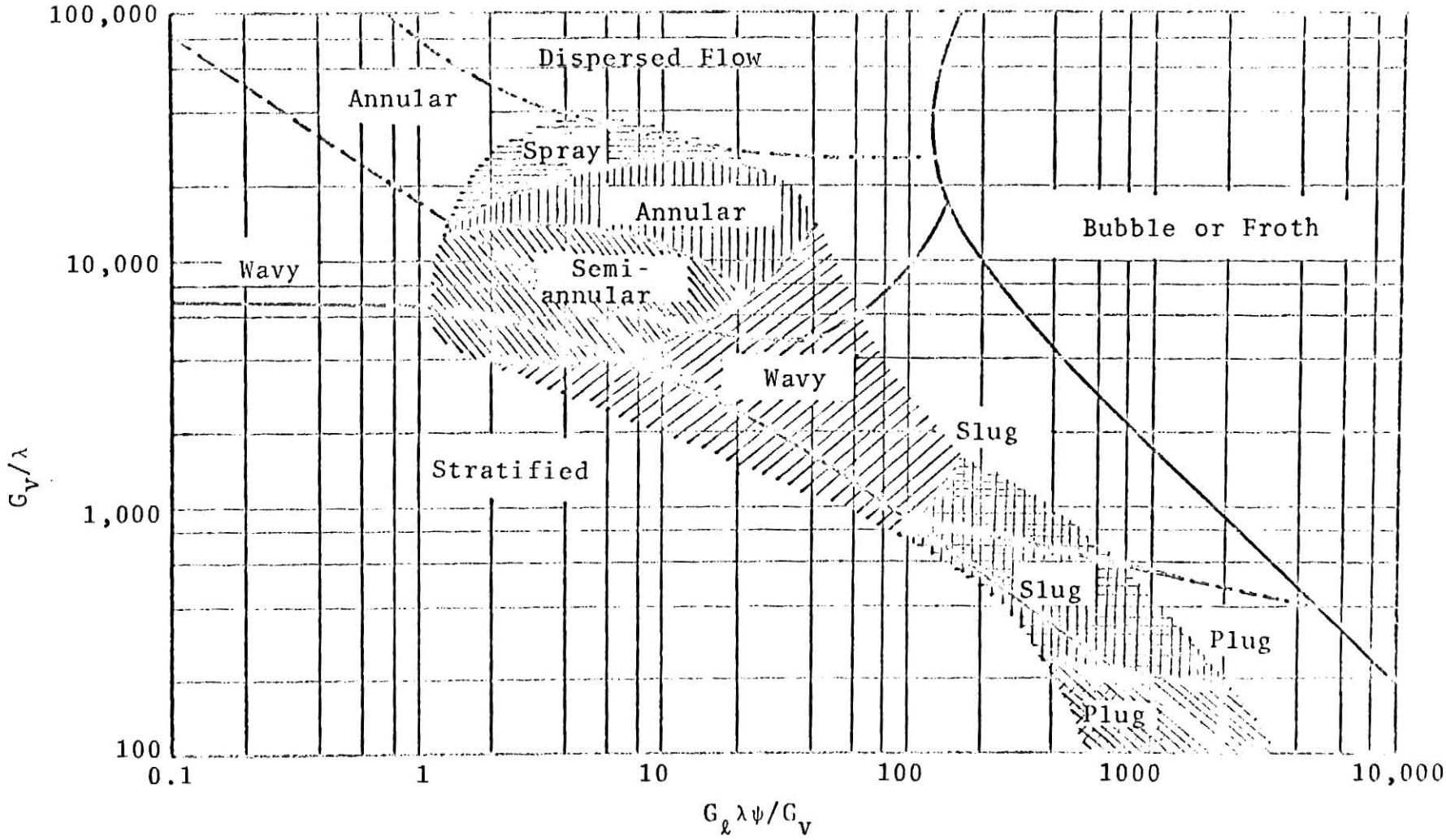

Fig. 14. A Comparison Between Flow Regime Areas of Condensation and Baker's [7] Flow Regime Areas of Adiabatic Two-Phase Flow.

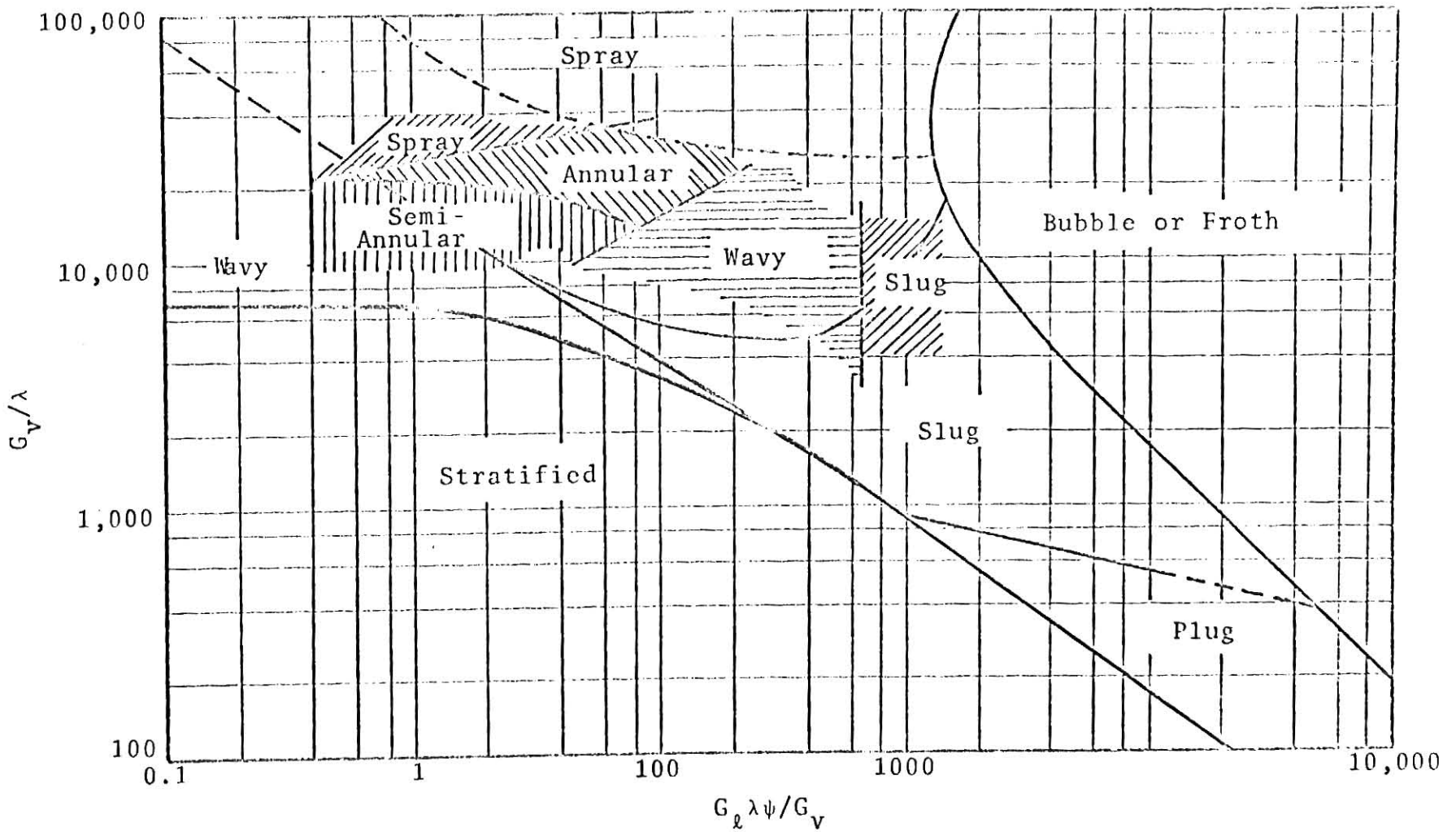

Fig. 15. Comparison Between Flow Regime Areas of Evaporation by Zahn [20,21] and Baker's [7] Flow Regime Areas of Adiabatic Two-Phase Flow

the vapor and liquid superficial velocities as coordinates. These flow maps have the disadvantage of being useless unless they are used to predict the flow patterns for systems similar to those that were used in constructing them. This is why Baker's [7] map or a map using Froude number and vapor volumetric ratios are preferable because of their more general use. The ordinates of the first map include parameters that depend on the properties of the two components (gas and liquid) of the flow. The latter has dimensionless coordinates. Figure 16 shows a flow pattern map constructed from the data of the present investigation using the vapor and liquid superficial velocities as coordinates. On the same figure the transition lines between the main flow patterns were arbitrarily drawn. Results of Fig. 16 indicate that if the superficial liquid velocity is maintained constant and the superficial vapor velocity is increased, the flow patterns develop in the following order: plug, slug, wavy, annular or semiannular, and spray. Increasing the vapor superficial velocity while maintaining the liquid superficial velocity constant is equivalent to increasing the quality of the condensing vapor. The main disadvantage of such a map is the fact that it cannot be generalized for use with other condensing fluids, or other condenser diameters.

Quandt [10] made a simplified analysis of adiabatic two-phase upflow and examined some of the controlling forces which influence the transition between two-phase flow patterns. He assumed that all flow regimes are controlled by the same forces, namely: pressure gradient forces, gravitational forces, and surface tension

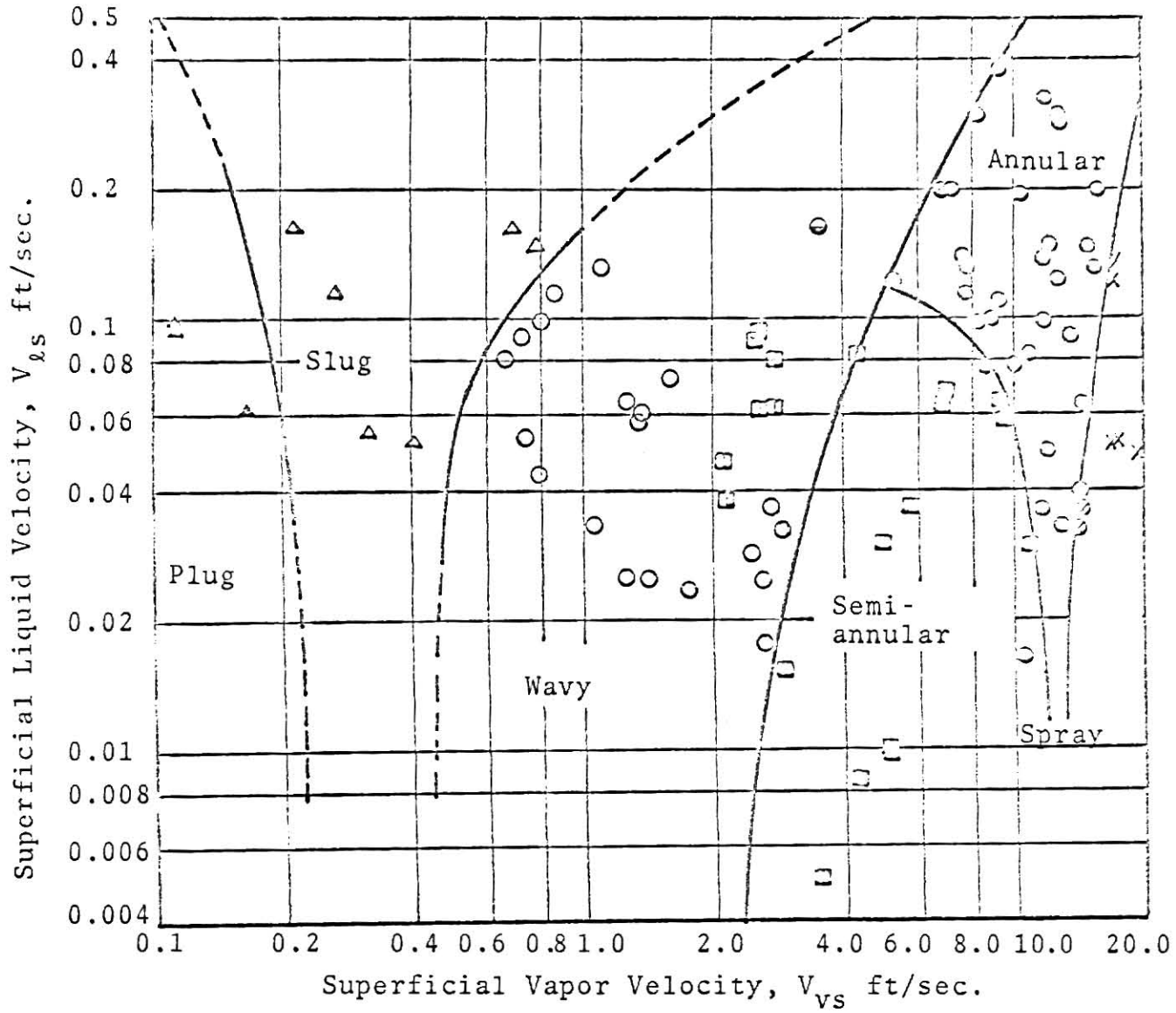

Fig. 16. Flow Regime Map Using Vapor and Liquid Superficial Velocities as Coordinates.

forces. Certain flow patterns occur when certain forces dominate the flow. For example, annular, spray, and bubbly flow patterns occur when the pressure gradient force dominates the other two forces. On the other hand, slug, wavy, and straitified flow patterns occur when the gravitational force dominates the flow. Quandt's [10] analysis lead to the following criteria for transition between pressure gradient controlled and gravity controlled regimes in horizontal channels:

$$N_{FR} = \frac{2}{f_{TP}} \frac{\rho_\ell}{\rho_{av}} \tag{1}$$

where f_{TP} is a friction factor for the two-phase mixture and ρ_{av} is the average mixture density given by:

$$\rho_{av} = \frac{1}{\frac{x}{\rho_v} + \frac{1-x}{\rho_\ell}} \tag{2}$$

Combining Eqns. (1) and (2), it can be shown that:

$$G^2 = \frac{2}{f_{TP}} gD \frac{\rho_\ell}{\frac{x}{\rho_v} + \frac{1-x}{\rho_\ell}} \tag{3}$$

Equation (3) can be used in constructing a transition line between pressure gradient controlled and gravity controlled flow regimes, on a flow pattern map, using G and x as parameters. Within the gravity controlled region, Quandt [10] described the transitions between slug and wavy flow by the following criterion:

$$N_{FR} = \frac{2}{f} \tag{4}$$

where f is a single-phase friction factor. It can be shown that Eqn. (4) can be written as follows:

$$G^2 = \frac{2}{f} \frac{gD}{\left(\frac{x}{\rho_v} + \frac{1-x}{\rho_\ell}\right)^2} \tag{5}$$

Equation (5) can be used in constructing the transition line between slug and wavy flows on a flow pattern map, using G and x as coordinates. In constructing a flow pattern map for air-water mixtures, Quandt [10] arbitrarily assumed $f_{TP} = f = 0.02$ in Eqns. (4) and (5), respectively. In this investigation, Fig. 17 was constructed using Eqns. (4) and (5), and by arbitrarily assuming $f_{TP} = f = 0.2$. It represents a flow pattern map for Refrigerant -12 condensing inside a 0.50 in. I.D. horizontal tube at a pressure of 90 psia.

A flow pattern map also can be constructed for the results of this investigation using the mass velocity G and the dryness fraction x as coordinates. The transition lines of such a map can be generated from their corresponding lines on the flow pattern maps of Figs. 11-a and 11-b. This can be achieved from the following relations:

$$\left.\begin{aligned} N_{FR} &= \frac{(G_v/\rho_v + G_\ell/\rho_\ell)^2}{gD} \\ R &= \frac{G_v/\rho_v}{G_v/\rho_v + G_\ell/\rho_\ell} \\ G &= G_v + G_\ell \\ x &= G_v/G \end{aligned}\right\} \tag{6}$$

A flow pattern map, using G and x as coordinates, can be constructed from Figs. 11-a and 11-b only if the tube diameter and the condensation pressure are specified. For the sake of comparison,

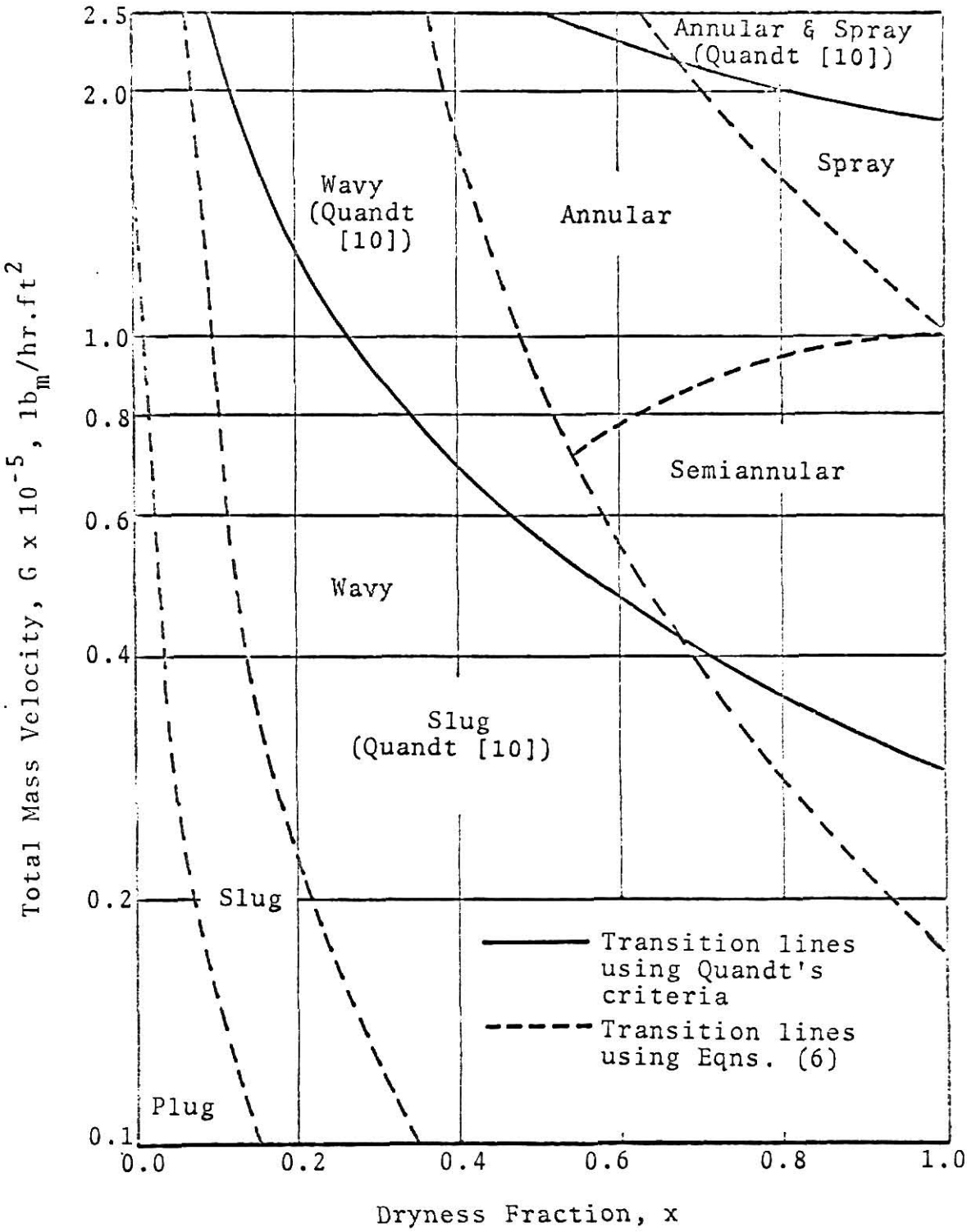

Fig. 17. Flow Pattern Map Using Mass Velocity and Dryness Fraction as Coordinates.

transition lines of Fig. 11-a and 11-b were reproduced in Fig. 17 by using Eqns. (6). They were plotted for Refrigerant-12 condensing inside a 0.50 inch I.D. horizontal tube at 90 psia. No meaningful conclusions could be made from the results of Fig. 18 for two reasons. First, Quandt [10] developed his criteria of transition for adiabatic two-phase flow. Second, the friction factors, f_{TP} and f, were arbitrarily chosen to plot Fig. 17.

A flow pattern map using G and x as coordinates has the disadvantage that it would be limited to certain tube diameters and certain pressures. As a matter of fact, any flow pattern map having dimensional coordinates has a limited application. For example, Fig. 17 was plotted for a certain tube diameter and a certain condensing pressure. If the diameter or the pressure were changed, the transition lines would also change. This is due to the fact that the properties of the condensing fluid, particularly ρ_ℓ and ρ_v, change with the change of the pressure.

The Effect of Cooling Rate and Inlet Superheat on the Flow Patterns

To establish the effect of the rate of cooling on the development of the flow pattern during condensation, a group of runs having nearly the same mass velocity, working pressure, and inlet superheat were chosen and tabulated in Table I. These runs differ only in the rate of cooling applied to the test condenser between the vapor inlet and any particular visual section. The following observations can be made from the results of Table I:

(a) Comparing the observations at the visual section B

Table I

Effect of Heat Rate

Run	$G \times 10^{-5}$ $lb_m/hr.ft^2$	P psia	Inlet superheat °F	Rate of heat removal Btu/hr	Visual section	Flow pattern observed
23	1.767	128.2	73.0	6318	B	Annular
				9488	C	Annular
25	1.647	116.2	74.5	5125	B	Annular
				7497	C	Annular
30	1.686	121.2	68.9	3523	B	Spray-Annular
				5169	C	Annular
34	2.050	126.5	61.0	3823	B	Spray
				5546	C	Annular
42	2.195	124.0	63.7	6316	A	Spray
				9485	B	Annular
				12264	C	Annular

during runs 23 and 30, one observes that the flow pattern at that section varied from spray-annular to annular when the rate of heat removal was increased from 3,523 to 6,319 Btu/hr.

(b) The flow pattern, at visual section B, during runs 34 and 42 changed from spray to annular due to a change in the rate of heat removal from 3,823 to 9,485 Btu/hr.

(c) A comparison between run 25 on the one hand, and runs 30 and 34 on the other, indicates similar results to those reported in parts (a) and (b) above.

The above discussion suggests that the rate of cooling is one of the factors that affects the flow pattern development.

To establish the effect of the inlet superheat, a group of runs, having nearly the same mass velocity, working pressure, and rate of heat removal were chosen and tabulated in Table II. These runs differ only in the inlet superheat temperature of the vapor at the condenser inlet. The following observations can be made from the results listed in Table II:

(a) During run 5, the inlet superheat temperature was 105.7°F, and the observed flow patterns at the three successive visual sections were: semiannular-wavy, wavy, and wavy. An increase in the superheat temperature to 120.3°F during run 7 changed the sequence of flow patterns to semiannular, semiannular-wavy, and then wavy.

(b) Comparins runs 7 and 8 leads to a result similar to that

Table II

Effect of Inlet Superheat

Run No.	$G \times 10^{-5}$ $lb_m/hr.ft^2$	P psia	Inlet superheat °F	Rate of heat removal Btu/hr	Visual section	Flow pattern observed
5	0.327	94.5	105.7	1009	A	Semiannular-wavy
				2019	B	Wavy
				3030	C	Wavy
7	0.299	93.0	120.3	1060	A	Semiannular
				1590	B	Semiannular-wavy
				2652	C	Wavy
8	0.288	96.0	90.4	958	A	Wavy
				1917	B	Wavy
				2876	C	Plug

reported in part (a) above.

The general trend is that the increase in inlet superheat will move the flow pattern towards a single-phase vapor flow.

CHAPTER V

SUMMARY, CONCLUSIONS, AND RECOMMENDATIONS

Summary and Conclusions

Flow patterns were visually and photographically studied during condensation of Refrigerant-12 inside a 0.5 in. I.D. horizontal tube. A wide range of operating conditions was covered. The flow patterns were studied at three different transparent sections located at 20, 60, and 100 ins. from the vapor inlet. The results of this investigation may be summarized as follows:

1. Nine flow patterns could be identified during condensation. Six flow patterns were considered as major ones and those were: spray, annular, semiannular, wavy, slug, and plug flows. The other three were considered as transitions between the major ones. The transition flow patterns were: annular-wavy, semiannular-wavy, and spray-annular.
2. The nine flow patterns could be observed and identified visually. However, only the six major flow patterns were distinguishable after the high speed motion pictures were taken.
3. Four different flow pattern maps were constructed from the results of this investigation; namely:
   i. Flow pattern map using Froude number and vapor volumetric ratio as coordinates.
   ii. Flow pattern map using Baker's [7] parameters as

coordinates.

iii. Flow pattern map using the superficial velocities of the liquid and the vapor as coordinates.

iv. Flow pattern map using the total mass velocity and the quality as coordinates.

When the first flow pattern map was compared with the one developed by Zahn [20,21] for evaporating Refriger-and-22, the agreement was fair. However, when the results of the present investigation were plotted on Baker's [7] map, which was developed for adiabatic two-phase flow, the agreement was poor. A similar result was observed by Zahn [20,21]. Such a result indicates that the flow pattern map of Baker, developed for adiabatic two-phase flow, is inadequate for diabatic two-phase flow. A new flow pattern map, using Baker's parameters was developed. It differs from Baker's original map in the location of the boundaries between the different flow patterns. The remaining two flow pattern maps could not be compared with similar maps due to the fact that no such maps are available in the literature for condensation.

4. The rate of heat removal and the inlet superheat had an effect on the development of the flow pattern during condensation. Their effect was demonstrated qualitatively by the results of this investigation.

5. The flow pattern map developed by using the Froude number and gas volumetric ratio, as coordinates, can be

considered as the most general one, among the ones developed from this investigation. Its coordinates reflect the effect of the various significant parameters, namely: the condensation pressure, the mass velocity, the quality, and the condenser's diameter. In addition, the physical interpretations of Froude number and the gas volumetric ratio seem to be compatible with the boundaries between the major flow patterns.

Recommendations for Further Studies

The attempt was made in this investigation to develop a flow pattern map for condensation inside a horizontal tube. Four flow pattern maps were developed from the results of this investigation. Different coordinates, used by other investigators, were used in constructing these maps. The flow pattern map constructed by using Froude number and gas volumetric ratios seemed to be the most general one because both coordinates used are dimensionless and reflect the effect of the various parameters, namely: the condensation pressure, the mass velocity, the tube diameter, and the vapor quality. It is recommended that the general use of such a map be verified by performing similar studies using different refrigerants and tube diameters. If the general use of such maps is established, all the empirical and semi-empirical correlations available in the literature for predicting the heat transfer coefficients and the pressure drop during condensation, should be reevaluated to determine the flow pattern to which they can be applied.

ACKNOWLEDGMENTS

The author wishes to express his deep appreciation to his major professor, Dr. N. Z. Azer, for his sincere and continuous help at different phases of this work. The direction and consultation of professors Wilson Tripp, J. E. Kipp, and C. Hsu have led to the author's gratitude. Recognition is also given to the American Society of Heating, Refrigerating, and Air Conditioning Engineering for their support of the experimental work.

The author is grateful for the free education offered to him in his home country, Egypt, and the willing sacrifice and continuous encouragement of his family during his graduate study.

SELECTED BIBLIOGRAPHY

1. Alves, G. E.
Concurrent Liquid-Gas Flow in a Pipe Contactor. Chem. Engg. Prog. 50 (1954) pp 449-456.

2. Martinelli, R. C., L. M. K. Boelter, T. H. M. Taylor, E. G. Thomsen, and E. H. Morrin.
Isothermal Pressure Drop for Two-Phase Two-Component Flow in a Horizontal Pipe. Trans. A.S.M.E. 66 (1944) pp 139-144.

3. Martinelli, R. C., J. A. Putnam, and R. W. Lockhart.
Two-Phase, Two-Component Flow in the Viscous Region, Trans. A.I.Ch.E. 42 (1946) p 681.

4. Lockhart, R. W., and R. C. Martinelli.
Proposed Correlation of Data for Isothermal Two-Phase Two-Component Flow in Pipes. Chem. Engg. Prog. 45 (1949) pp 39-48.

5. Bergelin, O. P., and C. Gazley.
Cocurrent Gas-Liquid Flow, I-Flow in Horizontal Tubes. Heat Transfer and Fluid Mechanics Institute, Berkeley, Calif. (1949) pp 5-19.

6. Hoogendoorn, C. J.
Gas-Liquid Flow in Horizontal Pipes. Chem. Engg. Sci. 9 (1959) pp 205-218.

7. Baker, O.
Simultaneous Flow of Oil and Gas. Oil and Gas J. 53 (1954) pp 185-195.

8. Goldmann, K., H. Fristenberg, and C. Lombardi.
Burnout in Turbulent Flow - A Droplet Diffusion Model. Trans. A.S.M.E. 83 (1961) pp 158-162.

9. Johnson, H. A., and A. H. Abou-Sabe.
Heat Transfer and Pressure Drop for Turbulent Flow of Air-Water Mixtures in a Horizontal Pipe. Trans. A.S.M.E. 74 (1952) pp 977-987.

10. Quandt, E.
Analysis of Gas-Liquid Flow Patterns. Chem. Engg. Prog. Symp., Ser. 57, 61 (1965) pp 128-135.

11. Berenson, P. J., and R. A. Stone.
A Photographic Study of the Mechanism of Forced Convection Vaporization. Chem. Engg. Prog. Symp., Ser. 57, 61 (1965) pp 213-219.

12. Sheinin, B. I., and A. K. Katarzhis.
Regimes of Forms of Flow of a Steam-Water Mixture in an Inclined Pipe. U.S. Atomic Energy Commission, AEC-tr-4496 (1959) pp 37-50.

13. Hosler, E. R.
Flow Patterns in High Pressure Two-Phase (Steam-Water) Flow With Heat Addition. Chem. Engg. Prog. Symp., Ser. 82, 64 (1968) pp 54-66.

14. Hosler, E. R.
Visual Study of Boiling at High Pressure. Chem. Engg. Prog. Symp., ser. 57, 61 (1965) pp 269-279.

15. Staub, F. W., and N. Zuber.
Void Fraction Profiles, Flow Mechanisms, and Heat Transfer Coefficients for Refrigerant-22 Evaporating in a Vertical Tube. ASHRAE Trans., 72, part I (1966) pp 130-146.

16. Hsu, Y. Y., and R. W. Graham.
A Visual Study of Two-Phase Flow in a Vertical Tube With Heat Addition. NASA Technical Notes, NASA TN D-1564 (1964).

17. Vohr, J. H.
Flow Patterns of Two-Phase Flow - A Survey of Literature. U.S. Atomic Energy Commission, TID-11514 (1960).

18. Vohr, J. H.
A Photographic Study of Boiling Flow. U.S. Atomic Energy Commission, NYO-9650 (1963).

19. Suo, M., A. E. Bergles, E. F. Doyle, L. Clawson, and P. Goldberg.
Investigation of Boiling Flow Regimes and Critical Heat Flux. U.S. Atomic Energy Commission, NYO-3304-3 (1965).

20. Zahn, W. R.
A Visual Study of Two-Phase Flow While Evaporating in Horizontal Tubes. Trans. A.S.M.E. 86, per. C (1964) pp 417-429.

21. Zahn, W. R.
Flow Conditions When Evaporating Refrigerant-22 in Air Conditioning Coils. ASHRAE Trans. 72, part I (1966) pp 82-89.

22. Bergles, A. E., and M. Suo.
Investigation of Boiling Water Flow Regimes at High Pressure. Proceedings of the 1966 Heat Transfer and Fluid Mechanics Institute, Calif. (1966) pp 79-99.

23. Griffith, P.
The Slug-Annular Flow Regime Transition at Elevated Pressure. Argonne National Laboratory, ANL-6796 (1963).

24. Abis, L. V.
Forced Convection Condensation Inside Horizontal Tubes. Ph. D. Dissertation, Kansas State University (1969).

25. American Society of Heating, Refrigerating and Air-Conditioning Engineering.
Thermodynamic Properties of Refrigerants. ASHRAE (1969).

APPENDICES

APPENDIX A

NOMENCLATURE

Symbol	Definition
Cp_w	water specific heat, Btu/lb_m°R
D	tube diameter, ft
g	gravitational acceleration, ft/sec^2
g_c	correction factor, 32.19 $lb_m ft/lb_f sec^2$
G	total mass velocity of Refrigerant-12, $lb_m/hr.ft^2$
G_v	vapor mass velocity, $lb_m/hr.ft^2$
G_ℓ	liquid mass velocity, $lb_m/hr.ft^2$
M_f	total mass flow rate of Refrigerant-12, lb_m/hr.
M_v	vapor mass flow rate, lb_m/hr.
M_ℓ	liquid mass flow rate, lb_m/hr.
M_w	cooling water mass flow rate, lb_m/hr.
N_{FR}	Froude number = $\frac{(V_{vs} + V_{\ell s})^2}{gD}$
N_{WE}	Weber number = $\frac{(V_s + V_{\ell s})^2 \rho_{av} D}{g_c \sigma}$
P	saturation pressure, psia
Q_v	vapor volume flow rate, ft^3/hr.
Q_ℓ	liquid volume flow rate, ft^3/hr.
R	gas volumetric ratio = $\frac{Q_v}{Q_\ell + Q_v}$
T_s	Refrigerant-12 saturation temperature, °F
V_{vs}	superficial vapor velocity, ft/sec
$V_{\ell s}$	superficial liquid velocity, ft/sec

x dryness fraction

x_A dryness fraction at visual section A

x_B dryness fraction at visual section B

x_C dryness fraction at visual section C

ρ_v saturated vapor density, lb_m/ft^3

ρ_ℓ saturated liquid density, lb_m/ft^3

ρ_{av} average mixture density, lb_m/ft^3

μ saturated liquid viscosity, centi-poise or $lb_m/ft.hr$

σ liquid surface tension, dyne/cm

λ Baker's [7] parameter = $\sqrt{(\rho_v/0.075)(\rho_\ell/62.3)}$

ψ Baker's [7] parameter = $(73/\sigma)[\mu_\ell(62.3/\rho_\ell)^2]^{1/3}$

ΔT_a cooling water temperature rise across condenser a, °F

ΔT_b cooling water temperature rise across condenser b, °F

ΔT_c cooling water temperature rise across condenser c, °F

APPENDIX B

TABLE B-1: OPERATING CONDITIONS AND HEAT BALANCE

Run No.	P	T_s	Inlet superheat	M_f	M_w	$G \times 10^{-5}$	Heat rate gained by water	Heat rate lost by Refrigerant-12	Heat balance % error
	psia	°F	°F	$lb_m/hr.$	$lb_m/hr.$	$lb_m/hr.ft^2$	Btu/hr.	Btu/hr.	
1	104.9	84.0	112.0	172.0	2123.7	1.262	4810	5182	7.2
2	106.5	85.1	116.9	145.8	2323.6	1.069	5673	5213	- 8.8
3	104.3	83.6	105.6	162.4	2398.5	1.191	5021	5588	10.2
4	101.0	81.5	98.2	136.9	2273.6	1.004	4070	2667	-52.6
5	94.5	77.0	105.7	44.6	2248.6	0.327	3030	2943	- 3.0
6	96.0	78.1	96.7	163.8	2173.7	1.202	3911	3843	- 1.8
7	93.0	76.0	120.3	40.8	2348.6	0.299	2652	2791	5.0
8	96.0	78.1	90.4	39.3	2128.7	0.288	2876	2937	2.1
9	100.4	81.0	86.3	205.5	2048.8	1.507	5522	5874	6.0
10	93.1	76.0	112.2	136.1	2698.4	0.998	4861	5332	8.8
11	94.5	77.0	116.9	65.6	2673.4	0.481	4217	4425	4.7
12	90.3	74.0	102.6	25.7	2023.8	0.189	1827	1707	- 7.0
13	94.5	77.0	99.4	26.9	1958.8	0.197	1766	1934	8.7
14	96.0	78.1	99.9	167.1	2073.7	1.226	3269	3608	9.4
15	93.1	76.0	105.7	40.8	1958.8	0.299	2650	3076	13.9
16	101.0	81.5	112.7	114.1	1923.8	0.837	4773	5068	5.8
17	96.0	78.1	122.8	56.4	1858.9	0.413	3359	3895	13.8
18	94.5	77.0	105.2	40.7	1848.9	0.298	2916	3068	5.0
19	97.4	79.0	121.0	85.1	1199.3	0.624	3522	3687	4.5
20	106.5	85.1	125.1	70.0	1848.9	0.513	4843	4905	1.3
21	124.7	96.0	90.4	178.2	1798.9	1.307	8286	7342	-12.9
22	126.5	97.1	124.1	66.7	1748.9	0.489	5296	5043	- 5.0
23	128.2	98.0	73.0	241.0	1748.9	1.767	9488	9673	1.9
24	111.2	88.0	110.5	112.9	1670.0	0.828	6368	5877	- 8.4
25	116.2	91.0	74.5	224.6	1748.9	1.647	7497	7345	- 2.1

Table B-1: Continued

Run No.	P	T_s	Inlet superheat	M_f	M_w	$G \times 10^{-5}$	Heat rate gained by water	Heat rate lost by Refrigerant-12	Heat balance % error
	psia	°F	°F	$lb_m/hr.$	$lb_m/hr.$	$lb_m/hr.ft^2$	Btu/hr.	Btu/hr.	
26	116.2	91.0	125.8	73.8	1699.0	0.541	5362	5298	- 1.2
27	93.1	76.0	83.7	29.9	1564.0	0.219	1905	2186	12.9
28	108.0	86.0	105.9	155.3	774.5	1.139	4882	5087	4.0
29	112.9	89.0	74.6	199.6	539.7	1.464	4450	4816	7.6
30	121.2	94.0	68.9	229.9	559.7	1.686	5169	5685	9.1
31	126.5	97.1	83.8	165.1	499.7	1.211	4982	5325	6.4
32	98.9	80.0	95.1	49.0	1424.1	0.359	3223	3339	3.5
33	103.4	83.0	85.4	26.0	519.7	0.191	1873	1908	1.8
34	126.5	97.1	61.0	279.5	589.6	0.205	5546	5912	6.2
35	126.5	97.1	57.4	304.9	1624.0	2.236	9153	10270	10.9
36	126.5	97.1	53.4	292.2	1424.1	2.143	10176	9279	- 9.7
37	126.5	97.1	57.2	273.1	409.8	2.003	5630	6009	6.3
38	126.5	97.1	74.4	168.3	509.7	1.235	5283	5277	- 0.1
39	126.5	97.1	105.9	171.5	1649.0	1.258	8577	7417	-15.6
40	98.9	80.0	94.8	49.0	459.7	0.359	3109	3112	0.1
41	127.0	97.3	62.0	231.7	499.7	1.700	4973	5607	11.3
42	124.0	95.6	63.7	299.3	1748.9	2.195	12264	12454	1.5

TABLE B-2: THERMOPHYSICAL PROPERTIES AND BAKER'S [7] FLOW PARAMETERS

Run No.	Vapor density, lb_m/ft^3 ρ_v	Liquid density, lb_m/ft^3 ρ_ℓ	Liquid viscosity, $lb_m/ft.hr$ μ_ℓ	Liquid surface tension, dyne/cm σ	Baker's [7] parameter λ	Baker's [7] parameter ψ
1	2.634	80.929	0.610	8.518	6.754	4.548
2	2.663	80.797	0.609	8.446	6.786	4.587
3	2.622	80.982	0.611	8.546	6.741	4.532
4	2.560	81.264	0.614	8.698	6.673	4.450
5	2.441	81.883	0.621	9.008	6.539	4.293
6	2.469	81.700	0.619	8.935	6.570	4.329
7	2.414	81.967	0.622	9.082	6.508	4.257
8	2.469	81.700	0.619	8.935	6.570	4.329
9	2.549	81.319	0.615	8.728	6.660	4.435
10	2.416	81.958	0.622	9.077	6.510	4.259
11	2.441	81.833	0.621	9.008	6.539	4.293
12	2.366	82.212	0.625	9.217	6.451	4.193
13	2.441	81.833	0.621	9.008	6.539	4.293
14	2.469	81.700	0.619	8.935	6.570	4.329
15	2.416	81.958	0.622	9.077	6.510	4.259
16	2.560	81.264	0.614	8.698	6.673	4.450
17	2.469	81.700	0.619	8.935	6.570	4.329
18	2.441	81.833	0.621	9.008	6.539	4.293
19	2.494	81.577	0.618	8.868	6.599	4.362
20	2.663	80.797	0.609	8.446	6.786	4.587
21	3.018	79.331	0.593	7.678	7.159	5.065
22	3.055	79.192	0.592	7.606	7.196	5.114
23	3.090	79.059	0.591	7.538	7.231	5.163
24	2.753	80.404	0.604	8.238	6.883	4.708
25	2.848	80.005	0.600	8.028	6.983	4.836
26	2.848	80.005	0.600	8.028	6.983	4.836
27	2.416	81.958	0.622	9.077	6.510	4.259
28	2.692	80.671	0.607	8.380	6.817	4.625
29	2.784	80.272	0.603	8.168	6.916	4.749
30	2.948	79.603	0.596	7.818	7.087	4.970
31	3.055	79.192	0.592	7.606	7.196	5.114
32	2.521	81.448	0.616	8.798	6.629	4.398
33	2.605	81.058	0.612	8.587	6.723	4.510
34	3.055	79.192	0.592	7.606	7.196	5.114
35	3.055	79.192	0.592	7.606	7.196	5.114
36	3.055	79.192	0.592	7.606	7.196	5.114
37	3.055	79.192	0.592	7.606	7.196	5.114
38	3.055	79.192	0.592	7.606	7.196	5.114
39	3.055	79.192	0.592	7.606	7.196	5.114
40	2.521	81.448	0.616	8.798	7.629	4.398
41	3.065	79.154	0.591	7.587	7.206	5.128
42	3.004	79.386	0.594	7.706	7.144	5.046

TABLE B-3: FLOW MAPS PARAMETERS

Run No.	Visual section	x	M_ℓ	M_v	$G_\ell \times 10^{-5}$	$G_v \times 10^{-5}$	$\frac{G_\ell \lambda \psi}{G_v}$	$\frac{G_v \times 10^{-4}}{\lambda}$	Flow patterns observed
			$lb_m/hr.$	$lb_m/hr.$	$lb_m/hr.ft^2$	$lb_m/hr.ft^2$			
1	C	0.81	32.5	139.6	0.238	1.024	7.14	1.515	annular
2	C	0.73	38.9	106.9	0.285	0.784	11.32	1.156	annular
3	B	0.91	14.4	148.0	0.105	1.085	2.97	1.610	annular
	C	0.72	45.5	116.9	0.333	0.857	11.88	1.272	annular
4	C	0.95	6.5	130.4	0.048	0.956	1.49	1.433	annular
5	A	0.95	2.1	42.5	0.016	0.312	1.41	0.477	semiannular
	B	0.57	19.1	25.5	0.140	0.187	21.01	0.286	wavy
	C	0.19	36.1	8.5	0.265	0.062	118.80	0.096	wavy
6	C	0.88	19.7	144.2	0.144	1.057	3.88	1.609	annular
7	A	0.85	6.2	34.6	0.045	0.254	4.95	0.390	semiannular
	B*	0.63	15.1	25.7	0.111	0.188	16.25	0.290	semiannular-wavy
	C	0.19	32.9	7.9	0.241	0.058	115.40	0.089	wavy
8	A	0.82	7.0	32.3	0.051	0.237	6.14	0.361	wavy
	B	0.41	23.1	16.2	0.170	0.118	40.69	0.181	wavy
	C	0.00	39.3	0.0	0.288	0.000	170600.00	0.000	plug
9	B	0.88	25.4	180.0	0.187	1.320	4.17	1.982	annular
	C	0.76	48.9	156.5	0.359	1.148	9.23	1.724	annular
10	B	0.81	25.6	110.5	0.188	0.810	6.43	1.244	semiannular
	C	0.66	44.0	90.1	0.338	0.660	14.17	1.015	annular
11	A	0.82	12.0	53.7	0.088	0.394	6.26	0.602	semiannular
	B	0.51	32.2	33.4	0.236	0.245	27.09	0.375	semiannular-wavy
	C	0.20	52.5	13.1	0.385	0.096	112.30	0.147	wavy

*Photographed flow pattern.

Table B-3: Continued

Run No.	Visual section	x	M_ℓ	M_v	$G_\ell \times 10^{-5}$	$G_v \times 10^{-5}$	$\frac{G_\ell \lambda \psi}{G_v}$	$\frac{G_v \times 10^{-4}}{\lambda}$	Flow patterns observed
			$lb_m/hr.$	$lb_m/hr.$	$lb_m/hr.ft^2$	$lb_m/hr.ft^2$			
12	B	0.48	13.5	12.2	0.099	0.090	29.78	0.139	wavy
	C	0.18	21.1	4.6	0.155	0.034	123.70	0.052	slug
13	A	0.63	10.1	16.8	0.074	0.123	16.85	0.189	wavy
	B	0.35	17.5	9.4	0.128	0.069	52.34	0.105	wavy
	C*	0.07	24.9	2.0	0.183	0.014	355.50	0.022	plug
14	C	0.92	13.1	154.0	0.096	1.129	2.42	1.719	annular
15	A	0.76	9.8	31.0	0.072	0.227	8.78	0.349	wavy
	B	0.40	24.6	16.1	0.181	0.118	42.30	0.182	wavy
	C	0.03	39.4	1.3	0.289	0.010	831.80	0.015	plug
16	B	0.77	26.7	87.3	0.196	0.641	9.09	0.960	semiannular
	C	0.57	48.9	65.2	0.359	0.478	22.27	0.716	annular
17	A	0.94	3.4	53.0	0.025	0.388	1.82	0.591	semiannular
	B	0.56	24.6	31.7	0.181	0.233	22.07	0.354	semiannular-wavy
	C	0.19	45.9	10.5	0.336	0.077	124.40	0.117	wavy
18	A	0.72	11.4	29.3	0.083	0.215	10.86	0.329	wavy
	B	0.38	25.4	15.3	0.186	0.112	46.43	0.172	wavy
	C	0.03	39.4	1.3	0.289	0.010	842.10	0.015	plug
19	B	0.83	14.4	70.7	0.105	0.518	5.86	0.786	semiannular
	C	0.62	32.7	52.3	0.240	0.384	17.99	0.582	semiannular-wavy
20	A	0.95	3.8	66.2	0.028	0.485	1.79	0.715	semiannular
	B	0.47	36.8	33.2	0.270	0.243	34.50	0.359	semiannular-wavy
	C	0.17	58.3	11.7	0.428	0.085	175.70	0.126	slug
21	B	0.83	30.3	147.9	0.222	1.085	7.42	1.515	annular
	C	0.57	76.4	101.8	0.560	0.747	27.19	1.043	annular

*Photographed flow pattern.

Table B-3: Continued

Run No.	Visual section	x	M_ℓ	M_v	$G_\ell \times 10^{-5}$	$G_v \times 10^{-5}$	$\frac{G_\ell \lambda \psi}{G_v}$	$\frac{G_v \times 10^{-4}}{\lambda}$	Flow patterns observed
			$lb_m/hr.$	$lb_m/hr.$	$lb_m/hr.ft^2$	$lb_m/hr.ft^2$			
22	B	0.64	24.2	42.5	0.177	0.312	20.94	0.433	semiannular-wavy
	C	0.05	63.5	3.2	0.466	0.023	736.00	0.032	slug
23	B	0.76	57.7	183.2	0.423	1.344	11.76	1.858	annular
	C	0.53	114.1	126.8	0.837	0.930	33.60	1.286	annular
24	B*	0.82	20.6	92.3	0.151	0.677	7.24	0.983	semiannular
	C	0.43	64.5	48.4	0.473	0.355	43.20	0.515	semiannular-wav
25	B	0.84	35.6	189.0	0.261	1.386	6.36	1.985	annular
	C	0.66	77.0	147.6	0.565	1.082	17.62	1.550	annular
26	A	0.95	4.0	69.8	0.029	0.512	1.92	0.733	semiannular
	B	0.49	37.4	36.4	0.274	0.267	34.70	0.382	semiannular-wavy
	C*	0.13	64.2	9.6	0.471	0.071	225.10	0.101	wavy-slug
27	A	0.68	9.5	20.4	0.069	0.150	12.82	0.230	wavy
	B	0.29	21.3	8.6	0.156	0.063	68.50	0.097	wavy
	C	0.01	29.6	0.3	0.217	0.002	2495.00	0.004	plug
28	B	0.92	11.7	143.6	0.086	1.053	2.58	1.544	semiannular
	C	0.75	38.8	116.5	0.285	0.854	10.51	1.253	annular
29	B	0.93	13.2	186.4	0.097	1.367	2.33	1.976	spray-annular
	C	0.81	38.6	161.0	0.283	1.180	7.88	1.707	annular
30	B	0.90	22.1	207.7	0.162	1.523	3.75	2.150	spray-annular
	C	0.78	51.1	178.8	0.375	1.311	10.06	1.850	annular
31	B	0.86	22.8	142.3	0.167	1.044	5.90	1.451	semiannular
	C	0.69	50.8	114.3	0.373	0.839	16.36	1.165	annular

*Photographed flow pattern.

Table B-3: Continued

Run No.	Visual section	x	M_ℓ	M_v	$G_\ell \times 10^{-5}$	$G_v \times 10^{-5}$	$\frac{G_\ell \lambda \psi}{G_v}$	$\frac{G_v \times 10^{-4}}{\lambda}$	Flow patterns observed
			$lb_m/hr.$	$lb_m/hr.$	$lb_m/hr.ft^2$	$lb_m/hr.ft^2$			
32	A	0.74	12.9	36.1	0.095	0.264	10.47	0.399	wavy
	B	0.40	29.3	19.7	0.215	0.144	43.48	0.218	wavy
	C	0.07	45.7	3.3	0.335	0.024	408.20	0.036	slug
33	A	0.62	10.0	16.0	0.073	0.118	18.92	0.175	wavy
	B	0.15	22.0	4.0	0.161	0.029	166.20	0.044	slug
	C	0.00	26.0	0.0	0.191	0.000		0.000	plug
34	B	0.93	20.2	259.3	0.148	1.901	2.87	2.642	spray
	C	0.82	50.8	228.7	0.373	1.677	8.18	2.331	annular
35	A	0.94	19.0	285.9	0.140	2.096	2.45	2.914	spray
	B	0.75	77.5	227.4	0.569	1.667	12.55	2.317	annular
	C	0.58	127.0	177.9	0.932	1.304	26.29	1.813	annular
36	B	0.84	47.8	244.3	0.351	1.792	7.21	2.490	spray
	C	0.61	114.3	177.8	0.839	1.309	23.66	1.813	annular
37	B	0.92	20.9	252.2	0.154	1.850	3.05	2.571	spray
	C	0.79	57.2	215.9	0.419	1.584	9.74	2.201	annular
38	B	0.86	23.3	145.0	0.171	1.064	5.91	1.478	semiannular
	C*	0.68	54.0	114.3	0.396	0.839	17.38	1.165	annular
39	B	0.83	29.8	141.7	0.218	1.039	7.74	1.444	annular
	C*	0.56	76.2	95.3	0.559	0.699	29.44	0.971	annular-wavy
40	A	0.70	14.9	34.1	0.109	0.250	12.75	0.377	wavy
	B	0.42	28.6	20.4	0.210	0.149	40.97	0.225	wavy
	C*	0.20	39.2	9.8	0.288	0.072	116.60	0.108	wavy

*Photographed flow pattern.

Table B-3: Continued

Run No.	Visual section	x	M_ℓ	M_v	$G_\ell \times 10^{-5}$	$G_v \times 10^{-5}$	$\frac{G_\ell \lambda \psi}{G_v}$	$\frac{G_v \times 10^{-4}}{\lambda}$	Flow patterns observed
			$lb_m/hr.$	lb_m/hr	$lb_m/hr.ft^2$	$lb_m/hr.ft^2$			
41	B*	0.93	15.7	216.0	0.115	1.584	2.68	2.199	spray-annular
	C	0.77	54.0	177.7	0.396	1.304	11.22	1.809	annular
42	A*	0.82	54.0	245.2	0.396	1.798	7.94	2.517	spray
	B	0.63	110.1	189.2	0.807	1.388	20.97	1.942	annular
	C	0.47	159.2	140.1	1.167	1.027	40.96	1.438	annular

*Photographed flow pattern.

TABLE B-4: FLOW MAPS PARAMETERS

Run No.	Visual section	Q_ℓ	Q_v	R	V_{vs}	$V_{\ell s}$	N_{FR}	N_{WE}	Flow patterns observed
		$ft^3/hr.$	$ft^3/hr.$		ft/sec	ft/sec			
1	C	0.401	52.993	0.993	10.80	0.082	88.21	845.36	annular
2	C	0.481	40.150	0.988	8.18	0.098	51.08	549.89	annular
3	B	0.178	56.450	0.997	11.50	0.036	99.22	843.56	annular
	C	0.562	44.591	0.988	9.08	0.114	63.08	672.63	annular
4	C	0.080	50.912	0.998	10.37	0.016	80.46	629.10	annular
5	A	0.026	17.411	0.999	3.55	0.005	9.41	67.73	semiannular
	B	0.234	10.455	0.978	2.13	0.048	3.53	41.52	semiannular-wavy
	C	0.441	3.495	0.888	0.71	0.090	0.48	15.29	wavy
6	C	0.241	58.397	0.996	11.90	0.049	106.39	842.84	annular
7	A	0.075	14.326	0.995	2.92	0.015	6.42	50.67	semiannular
	B	0.184	10.641	0.983	2.17	0.038	3.63	38.09	semiannular-wavy
	C	0.401	3.268	0.891	0.67	0.082	0.42	12.91	wavy
8	A	0.086	13.099	0.994	2.67	0.017	5.38	45.49	wavy
	B	0.283	6.553	0.959	1.34	0.058	1.45	23.59	wavy
	C	0.481	0.003	0.006	0.00	0.098	0.01	1.67	plug
9	B	0.313	70.635	0.996	14.39	0.064	155.75	1309.33	annular
	C	0.602	61.421	0.990	12.51	0.123	119.03	1144.60	annular
10	B	0.313	45.719	0.993	9.31	0.064	65.56	540.98	semiannular
	C	0.562	37.276	0.985	7.59	0.114	44.30	444.68	annular
11	A	0.146	21.982	0.993	4.48	0.030	15.15	126.40	semiannular
	B	0.394	13.682	0.972	2.79	0.080	6.13	80.40	semiannular-wavy
	C	0.642	5.377	0.893	1.10	0.131	1.12	34.38	wavy
12	B	0.164	5.175	0.969	1.05	0.033	0.88	11.68	wavy
	C	0.257	1.951	0.884	0.40	0.052	0.15	4.83	slug

Table B-4: Continued

Run No.	Visual section	Q_ℓ	Q_v	R	V_{vs}	$V_{\ell s}$	N_{FR}	N_{WE}	Flow patterns observed
		$ft^3/hr.$	$ft^3/hr.$		ft/sec	ft/sec			
13	A	0.123	6.888	0.982	1.40	0.025	1.52	16.42	wavy
	B	0.214	3.848	0.947	0.78	0.044	0.51	9.51	wavy
	C	0.305	0.807	0.726	0.16	0.062	0.04	2.60	plug
14	C	0.160	62.378	0.997	12.71	0.033	121.02	916.89	annular
15	A	0.120	12.811	0.991	2.61	0.024	5.17	45.52	wavy
	B	0.300	6.679	0.957	1.36	0.061	1.51	24.57	wavy
	C	0.481	0.544	0.531	0.11	0.098	0.03	3.61	plug
16	B	0.329	34.110	0.991	6.95	0.067	36.70	354.09	semiannular
	C	0.602	25.460	0.977	5.19	0.123	21.01	267.90	annular
17	A	0.042	21.455	0.998	4.37	0.009	14.30	106.29	semiannular
	B	0.301	12.854	0.977	2.62	0.061	5.36	65.05	semiannular-wavy
	C	0.562	4.247	0.883	0.87	0.114	0.72	23.78	wavy
18	A	0.139	12.020	0.989	2.45	0.028	4.57	43.06	wavy
	B	0.310	6.280	0.953	1.28	0.063	1.34	23.34	wavy
	C	0.481	0.538	0.528	0.11	0.098	0.03	3.61	plug
19	B	0.176	28.338	0.994	5.77	0.036	25.16	214.42	semiannular
	C	0.401	20.986	0.981	4.28	0.082	14.15	160.82	semiannular-wavy
20	A	0.047	24.849	0.998	5.06	0.010	19.18	161.73	semiannular
	B	0.455	12.465	0.965	2.54	0.093	5.17	83.93	semiannular-wavy
	C	0.722	4.380	0.859	0.89	0.147	0.81	33.14	slug
21	B	0.381	49.004	0.992	9.98	0.078	75.46	898.42	annular
	C	0.963	33.731	0.972	6.87	0.196	37.24	631.15	annular
22	B	0.306	13.914	0.979	2.83	0.062	6.26	97.74	semiannular-wavy
	C	0.802	1.040	0.565	0.21	0.163	0.11	12.66	slug
23	B	0.730	59.293	0.988	12.08	0.149	111.48	1504.20	annular
	C	1.444	41.037	0.966	8.36	0.294	55.84	1064.58	annular

Table B-4: Continued

Run No.	Visual section	Q_ℓ	Q_v	R	V_{vs}	$V_{\ell s}$	N_{FR}	N_{WE}	Flow patterns observed
		$ft^3/hr.$	$ft^3/hr.$		ft/sec	ft/sec			
24	B	0.256	33.510	0.992	6.83	0.052	35.28	362.66	semiannular
	C	0.802	17.569	0.956	3.58	0.163	10.44	197.31	semiannular-wavy
25	B	0.445	66.352	0.993	13.52	0.091	136.06	1465.11	annular
	C	0.963	51.819	0.982	10.56	0.196	86.20	1157.70	annular
26	A	0.050	24.513	0.998	4.99	0.010	18.67	177.02	semiannular
	B	0.468	12.779	0.965	2.60	0.095	5.43	95.46	semiannular-wavy
	C	0.802	3.380	0.808	0.69	0.163	0.54	30.14	slug
27	A	0.115	8.466	0.987	1.72	0.024	2.28	22.17	wavy
	B	0.260	3.567	0.932	0.73	0.053	0.45	9.89	wavy
	C	0.361	0.136	0.274	0.03	0.074	0.01	1.28	plug
28	B	0.146	53.335	0.997	10.87	0.030	88.50	776.99	semiannular
	C	0.481	43.272	0.989	8.82	0.098	59.23	635.67	annular
29	B	0.165	66.938	0.998	13.64	0.034	139.33	1285.51	spray-annular
	C	0.481	57.812	0.992	11.78	0.098	105.15	1116.74	annular
30	B	0.278	70.457	0.996	14.35	0.057	154.82	1630.37	spray-annular
	C	0.642	60.636	0.990	12.35	0.131	116.19	1412.41	annular
31	B	0.288	46.594	0.994	9.49	0.059	68.01	797.99	semiannular
	C	0.642	37.427	0.983	7.62	0.131	44.84	647.98	annular
32	A	0.159	14.301	0.989	2.91	0.032	6.47	63.13	wavy
	B	0.360	7.801	0.956	1.59	0.073	2.06	35.63	wavy
	C	0.562	1.296	0.698	0.26	0.114	0.11	8.11	slug
33	A	0.123	6.148	0.980	1.25	0.025	1.22	14.89	wavy
	B	0.271	1.540	0.950	0.31	0.055	0.10	4.30	slug
	C	0.321	0.003	0.008	0.00	0.065	0.00	0.77	plug
34	B	0.255	84.868	0.997	17.29	0.052	224.21	2452.03	spray
	C	0.642	74.853	0.992	15.25	0.131	176.35	2174.67	annular

Table B-4: Continued

Run No.	Visual section	Q_ℓ	Q_v	R	V_{vs}	$V_{\ell s}$	N_{FR}	N_{WE}	Flow patterns observed
		$ft^3/hr.$	$ft^3/hr.$		ft/sec	ft/sec			
35	A	0.240	93.574	0.997	19.06	0.049	272.32	2948.03	spray
	B	0.979	74.426	0.987	15.16	0.199	175.94	2369.55	annular
	C	1.604	58.219	0.973	11.86	0.327	110.74	1879.90	annular
36	B	0.604	79.985	0.993	16.29	0.123	200.96	2426.92	spray
	C	1.444	58.219	0.976	11.86	0.294	110.14	1796.74	annular
37	B	0.264	82.557	0.997	16.82	0.054	212.25	2331.51	spray
	C	0.722	70.695	0.990	14.40	0.147	157.82	2010.44	annular
38	B	0.294	47.480	0.994	9.67	0.060	70.62	828.83	semiannular
	C	0.682	37.427	0.982	7.62	0.139	44.94	661.14	annular
39	B	0.376	46.390	0.992	9.45	0.077	67.67	826.64	annular
	C	0.963	31.189	0.970	6.35	0.196	31.99	568.31	annular-wavy
40	A	0.183	13.520	0.987	2.75	0.037	5.81	59.82	wavy
	B	0.352	8.080	0.958	1.65	0.072	2.20	36.81	wavy
	C	0.481	3.887	0.890	0.79	0.098	0.59	19.07	wavy
41	B	0.198	70.487	0.997	14.36	0.040	154.60	1692.60	spray-annular
	C	0.682	58.000	0.988	11.82	0.139	106.54	1405.12	annular
42	A	0.681	81.630	0.992	16.63	0.139	209.64	2506.12	spray
	B	1.386	62.980	0.979	12.83	0.282	128.21	1959.84	annular
	C	2.005	44.630	0.959	9.50	0.409	73.19	1480.82	annular

APPENDIX C

CALCULATIONS SAMPLE FOR RUN NUMBER 16

Recorded Data

The following readings were recorded for Run 16:

Reference (ambient) temperature	= 82°F
Atmospheric pressure	= 14.7 psi
Condenser inlet pressure	= 86.9 psig
Condenser exit pressure	= 85.7 psig
Refrigerant-12 inlet temperature	= 2.73 m.v.
Refrigerant-12 exit temperature	= -0.12 m.v.
Condensate flow rate at exit	= 0.075 gpm
Condensed vapor flow rate	= 0.100 gpm
Water inlet temperature of condenser c	= -0.510 m.v.
Water exit temperature of condenser c	= -0.495 m.v.
Water inlet temperature of condenser b	= -0.495 m.v.
Water exit temperature of condenser b	= -0.475 m.v.
Water inlet temperature of condenser a	= -0.475 m.v.
Water exit temperature of condenser a	= -0.455 m.v.
Water flow rate through the condenser	= 3.85 gpm

The observed flow patterns of this run, at the three visual sections, A, B, and C are listed in Tables B-3 and B-4.

Step 1: Thermophysical Properties and Flow Parameters

The working pressure for this run was assumed as the average between the inlet and exit values, then

$$P = \frac{86.9 + 85.7}{2}$$

$$= 86.3 \text{ psig}$$

$$= 101 \text{ psia}$$

All properties were taken from reference [24], consequently

T_s = 81.5°F

ρ_v = 2.560 lb_m/ft^3

ρ_ℓ = 81.264 lb_m/ft^3

μ_ℓ = 0.614 $lb_m/ft.hr$

σ = 8.698 dyne/cm

Saturated vapor enthalpy = 85.43 Btu/lb_m

Saturated liquid enthalpy = 26.75 Btu/lb_m

$$\lambda = \sqrt{\left(\frac{2.560}{0.075}\right)\left(\frac{81.264}{62.3}\right)}$$

$$= 6.673$$

1 $lb_m/hr.ft$ = 0.414 centi-poise

$$\mu_\ell = 0.614 \times 0.414$$

$$= 0.2545 \text{ centi-poise}$$

$$\psi = \frac{73}{8.698}\left[0.2545\left(\frac{62.3}{81.264}\right)^2\right]^{1/3}$$

$$= 4.450$$

Step 2: Heat Balance Error

$$M_f = (0.075 + 0.100) \frac{\text{gallons}}{\text{minute}} \times 60 \frac{\text{minutes}}{\text{hour}} \times 0.13368 \frac{ft^3}{\text{gallon}}$$

$$\times 81.264 \frac{lb_m}{ft^3}$$

$$= 114.1 \text{ } lb_m/hr$$

$$M_w = 3.85 \frac{\text{gallons}}{\text{minute}} \times 60 \frac{\text{minutes}}{\text{hour}} \times 0.13368 \frac{\text{ft}}{\text{gallon}} \times 62.3 \frac{lb_m}{ft^3}$$

$$= 1923.8 \ lb_m/hr$$

$$G = \frac{114.1}{\frac{\pi}{4}(\frac{0.5}{12})^2} = 0.837 \times 10^5 \ lb_m/hr.ft^2$$

Conversion of Temperature Measurements From m.v. into °F

Refrigerant-12 inlet temperature = 1.94.2°F

ΔT_c = 0.683°F

ΔT_b = 0.907°F

ΔT_a = 0.878°F

$x_c = \frac{0.100}{0.175}$

= 0.57

The mixture enthalpy at condenser exit

= 0.57(85.43) + 0.43(26.75)

= 60.3 Btu/lb_m

Enthalpy of refrigerant at inlet = 104.7 Btu/lb_m

Heat lost by refrigerant = 114.1(104.7 - 60.3)

= 5068 Btu/hr

Total water temperature difference across the condenser

= 2.468°F

Heat gained by water = 1923.8 × 2.468 × 0.999

= 4773 Btu/hr

Percentage heat balance error = $\frac{5068 - 4773}{5068} \times 100$

= 5.8%

Step 3: Flow Pattern Parameters at Each Visual Section

Visual Section C

$$M_V = 0.57 \times 114.1$$

$$= 65.2 \text{ lb}_m/\text{hr}$$

$$M_\ell = 0.43 \times 114.1$$

$$= 48.9 \text{ lb}_m/\text{hr}$$

$$G_V = 65.2/\frac{\pi}{4}\left(\frac{0.5}{12}\right)^2$$

$$= 0.478 \times 10^5 \text{ lb}_m/\text{hr.ft}^2$$

$$G_\ell = 48.9/\frac{\pi}{4}\left(\frac{0.5}{12}\right)^2 = 0.359 \times 10^5 \text{ lb}_m/\text{hr.ft}^2$$

$$\frac{G_\ell \lambda \psi}{G_V} = \frac{0.359 \times 10^5 \times 6.673 \times 4.45}{0.478 \times 10^5}$$

$$= 22.27$$

$$\frac{G_V}{\lambda} = \frac{0.478 \times 10^5}{6.673}$$

$$= 7.163 \times 10^3$$

$$Q_V = \frac{M_V}{\rho_V}$$

$$= \frac{65.2}{2.560}$$

$$= 25.460 \text{ ft}^3/\text{hr}$$

$$Q_\ell = \frac{M_\ell}{\rho_\ell}$$

$$= \frac{48.9}{81.264}$$

$$= 0.600 \text{ ft}^3/\text{hr}$$

$$R = \frac{25.460}{25.460 + 0.600} = 0.977$$

$$V_{vs} = \frac{25.460}{\frac{\pi}{4}(\frac{0.5}{12})^2(3600)}$$

$$= 5.19 \text{ ft/sec}$$

$$V_{\ell s} = \frac{0.600}{\frac{\pi}{4}(\frac{0.5}{12})^2(3600)}$$

$$= 0.123 \text{ ft/sec}$$

$$N_{FR} = \frac{(5.19 + 0.123)^2}{32.2(\frac{0.5}{12})}$$

$$= 21.01$$

$$\rho_{av} = \frac{1}{\frac{x}{\rho_v} + \frac{1-x}{\rho_\ell}}$$

$$= \frac{1}{\frac{0.57}{2.560} + \frac{0.43}{81.264}}$$

$$= 4.377 \text{ lb}_m/\text{ft}^3$$

$$1 \text{ dyne/cm} = 6.87 \times 10^{-5} \text{ lb}_f/\text{ft}$$

$$\sigma = 8.698 \times 6.87 \times 10^{-5}$$

$$= 5.98 \times 10^{-4} \text{ lb}_f/\text{ft}$$

$$N_{WE} = \frac{(5.19 + 0.123)^2(4.377)(0.5/12)}{32.2 \times 5.98 \times 10^{-5}}$$

$$= 267.9$$

Visual Section B

$$x_B = x_C + \frac{M_w Cp_w \Delta T_c}{M_f L}$$

where L = refrigerant latent heat in Btu/lb_m

$$x_B = 0.57 + \frac{1923.8 \times 0.999 \times 0.683}{114.1 \quad 58.68} = 0.77$$

The following can be calculated for Section B:

$M_v = 87.4\ lb_m/hr$

$M_\ell = 26.7\ lb_m/hr$

$G_v = 0.641 \times 10^5\ lb_m/hr.ft^2$

$G_\ell = 0.196 \times 10^5\ lb_m/hr.ft^2$

$\frac{G_\ell \lambda \psi}{G_v} = 9.09$

$\frac{G_v}{\lambda} = 0.960 \times 10^4$

$Q_v = 34.110\ ft^3/hr$

$Q_\ell = 0.329\ ft^3/hr$

$V_{vs} = 6.95\ ft/sec$

$V_{\ell s} = 0.067\ ft/sec$

$N_{FR} = 36.70$

$N_{WE} = 354.09$

$R = 0.991$

Visual Section A

$$x_A = x_C + \frac{M_w Cp_w (\Delta T_b + \Delta T_c)}{M_f L}$$

$$= 0.57 + \frac{1923.8 \times 0.999 \times (0.683 + 0.907)}{114.1 \times 58.68}$$

$$= 1.025$$

Such a result indicates that the vapor in Visual Section A was still superheated.

VISUAL AND PHOTOGRAPHIC FLOW PATTERN STUDIED DURING CONDENSATION INSIDE HORIZONTAL TUBES

by

HASSAN MOHAMED HASSAN SOLIMAN

B.Sc., Assiut University, U.A.R., 1966

AN ABSTRACT OF A MASTER'S THESIS

submitted in partial fulfillment of the

requirements for the degree

MASTER OF SCIENCE

Department of Mechanical Engineering

KANSAS STATE UNIVERSITY

Manhattan, Kansas

1970

ABSTRACT

Flow patterns were visually and photographically studied during condensation of Refrigerant-12 inside an 0.50 in. I.D. horizontal tube. A wide range of condensing conditions was covered. The flow patterns were studied at three different transparent sections located at 20, 60, and 100 ins. from the vapor inlet. Nine flow patterns were identified. Six of these flow patterns were considered as major ones and the remaining three were considered as transition patterns. The six major patterns were: spray, semiannular, annular, wavy, slug, and plug flows. The transition patterns were: semiannular-wavy, annular-wavy, and spray-annular flows. The nine flow patterns could be identified visually. However, only the major ones were distinguishable by the high speed movie pictures taken.

Four flow pattern maps were constructed from the results of this investigation as follows:

i) Flow pattern map using Froude number and the gas volumetric ratio as coordinates.

ii) Flow pattern map using Baker's parameters as coordinates.

iii) Flow pattern map using the liquid and the vapor superficial velocities as coordinates.

iv) Flow pattern map using the total mass velocity and the vapor quality as coordinates.

It was concluded that Baker's map developed for adiabatic two-phase flow was not adequate for predicting the flow patterns of diabatic two-phase flow in general and during condensation in

particular. The flow pattern map constructed by using Froude number and the vapor volumetric ratio as coordinates is being recommended for predicting the flow pattern during condensation. It is also recommended that the general use of such a map be verified by a similar study using different condensing refrigerants and other tube diameters. The effect of the rate of heat removal and the inlet superheat on the development of the flow patterns was qualitatively established.